Accepted Manuscript

Nanocomposite Nb-Al-N coatings: Experimental and theoretical principles of phase transformations

Alexander Pogrebnjak, Vladyslav Rogoz, Volodymyr Ivashchenko, Oleksandr Bondar, Volodymyr Shevchenko, Stefan Jurga, Emerson Coy

PII: S0925-8388(17)31730-9

DOI: 10.1016/j.jallcom.2017.05.136

Reference: JALCOM 41866

To appear in: *Journal of Alloys and Compounds*

Received Date: 7 February 2017

Revised Date: 3 May 2017

Accepted Date: 13 May 2017

Please cite this article as: A. Pogrebnjak, V. Rogoz, V. Ivashchenko, O. Bondar, V. Shevchenko, S. Jurga, E. Coy, Nanocomposite Nb-Al-N coatings: Experimental and theoretical principles of phase transformations, *Journal of Alloys and Compounds* (2017), doi: 10.1016/j.jallcom.2017.05.136.

Nanocomposite Nb-Al-N coatings: Experimental and Theoretical Principles of Phase Transformations

Alexander Pogrebnjak[1,*], Vladyslav Rogoz[1], Volodymyr Ivashchenko[2], Oleksandr Bondar[1], Volodymyr Shevchenko[2], Stefan Jurga[3], Emerson Coy[3]

1. Sumy State University, Department of nanoelectronics, 40007, R.-Korsakova 2, Sumy, Ukraine; e-mail: alexp@i.ua

2. Institute of Problems of Material Science, NAS of Ukraine, Krzhyzhanovsky 3, 03680, Kyiv-142, Ukraine

3. NanoBioMedical Centre, Adam Mickiewicz University, ul. Umultowska 85, 61614 Poznań, Poland

* - corresponding author

Abstract

Phase transformations of Al doped NbN nanocomposite coatings are studied in detail focusing on their microstructural evolution and phase composition. Several techniques such as XRD, SEM, HR-TEM, Nanoindentation and molecular dynamics simulation are employed in order to understand the phase evolution of the Nb-Al-N system. The nanocomposite structures were formed in the coatings, the roughness of the coatings decreased with increasing the Al concentration due to decreasing grain size. First-principles investigation of Nb-Al-N solid solutions was carried out to interpret film properties. It was found, that for small Al fractions, the solid solutions will form in agreement with our experimental results. The spinodal decomposition of Nb-Al-N solid solutions is supposed to be responsible for the formation of the nanocomosite structure observed in the deposited Nb-Al-N films.

Keywords: Nanocomposites, Metals and alloys, Mechanical properties, Computational modeling, Microstructure, C-PVD

Introduction

NbN based coatings are quite perspective for industrial application due to their high melting temperature, splendid physico-mechanical and superconducting properties [1–9]. Such coatings can be widely used for fabrication of Josephson's large integrated circuits [10–13], bolometers [10]–[15] and superconducting one-photon detectors [1,4,14–24]. Low thermal stability and oxidation resistance are among the main disadvantages of such coatings. Addition of impurities to the crystal lattice of the transition metal nitrides form nanostructured coatings with improved properties [25–32]. Ternary nitrides, such as $Ti_{1-x}Al_xN$, $Zr_{1-x}Al_xN$ and $Cr_{1-x}Al_xN$ have higher hardness, oxidation resistance and thermal stability in comparison with binary CrN, ZrN and TiN coatings [33–43]. Mainly, the mechanical and chemical properties of $Me_{1-x}Al_xN$ improve due to the increasing of Al concentration up to a critical value, when the B1 structure transforms into the B4 one. This leads to significant decreasing of hardness and wear resistance [40,42,44–46]. A formation of the two-phase structure B1+B4 leads to decreasing oxidation resistance [40,47–49].

Changes in the composition of $Nb_{1-x}Al_xN$ films are due to changing the Al content [50–53]. When $x \leq 0.08$, the mix of δ' (hexagonal)+δ (cubic B1, Fm3-m) phases forms [52]. When the Al concentration is in the range 50-53 %, the films have cubic B1-structure, with the (200) preferred plane of growth [50–53]. The 50-66% concentration of Al leads to the formation of B1-$Nb_{1-x}Al_xN$ with the B4 (wurtzite-type) -AlN structure [50–52,54]. When the concentration of Al is higher than 65%, a nanocomposite structure is formed with 20 nm B4-AlN crystallites [50].

To our knowledge, the Nb-Al-N films with a nanocomposite structure were not yet prepared, although we suppose that such films can be synthesized under certain conditions. To verify this assumption we have deposited Al-Nb-N films by magnetron sputtering at different currents supplied to the Al target. Deposited coatings were annealed at the temperature 1000 ^oC for one hour in order to check their thermal stability. To interpret coating structure, first-principles investigations of Nb-Al-N solid solutions were carried out.

Experimental details

Nb−Al−N coatings were deposited on mirror-polished Si (100) wafers by DC reactive magnetron sputtering using Nb (99.9 %, Ø 72 x 4 mm) and Al (99.999 %, Ø 72 x 4 mm) targets in an argon-nitrogen atmosphere. The deposition conditions were: substrate temperature T_S = 350 °C; substrate bias U_B = -50 V; flow rates F_{Ar} = 40 cm^3/min and F_{N2} = 13 cm^3/min; working pressure P = 0.17 Pa. The currents, applied to the Al target (I_{Al}) were 0, 50, 100, 150, 250 and 300 mA, which corresponded to discharge power densities P_{Al} = 0, 2.9, 5.7, 8.6, 13.7 and P_{Al} = 17.1 W/cm^2, respectively. The current, applied to the Nb target (I_{Nb}), was 300 mA (P_{Nb} = 17.1 W/cm^2). The base pressure inside the vacuum chamber was less than 10^{-4} Pa. The distance between the targets and the substrate holder was 8 cm. The dihedral angle between the target planes was around 45^0. The substrates were preliminary cleaned ultrasonically and were etched in the vacuum chamber in hydrogen plasma during 5 min before deposition. All deposition parameters for all samples are presented in the Table 1. Post-deposition vacuum annealing of the coatings at 600, 800 and 1000 °C was done.

Studies of the surface of the coatings were done using scanning atomic-force microscope Bruker's Innova in a half-contact mode and electron microscope JEOL 7001 F with SEI detector, the accelerating voltage was 15 kV. Structural and mechanical properties were determined in dependence on the currents applied to the Al target and annealing temperatures. Microstructure of the coatings was determined by X-ray diffraction (XRD, X'pert3 MRD (XL) from PANalytical) using CuKα radiation. PowderCell 2.4 software was used for profiles separation in the case of overlaying of the complex profiles. Substructural characteristics, such as size of crystallites and microdeformation, were determined using approximation method, Cauchy function was used as approximating function. Cross-sections of the samples were prepared by focused ion beam (FIB, JEOL JIB-4000). The cross-sections were then studied by high-resolution transmission electron microscopy JEOL-ARM 200F with an accelerating voltage 200 kV, equipped with an energy-dispersive X-ray spectroscopy (EDS) detector. The hardness of the coatings was determined from nanoindentation by Nanoindenter-G200 instrument, equipped with a Berkovich

pyramidal tip. The range of loads was chosen in order to obtain prominent plastic deformation of the coating while avoiding the influence of substrate material. Thus, the indenter's penetration depth did not exceed 10–20% of the total thickness of the coating. Microhardness measurements were done using REVETEST device (Switzerland), nanohardness and elastic modulus were studied using Triboindentor TI-950 (HYSITRON Inc.) in dynamic mode. Thickness of the coatings was determined by optical profilometer "Micron-gamma", and it was in the range of 0.7-0.9 μm.

Theoretical details

We performed first-principles investigation of Nb-Al-N solid solutions (alloys) to interpret our experimental results. In order to investigate Nb-Al-N solid solutions with the B1 structure (space group Fm-3m, No. 225) we considered cubic supercells $Nb_{32}N_{28}$, $Nb_{24}Al_8N_{29}$, $Nb_{16}Al_{16}N_{30}$, $Nb_8Al_{24}N_{31}$, $Al_{32}N_{32}$, representing special quasirandom structures (SQS) $Nb_{1-x}Al_xN_{(7+x)/8}$ [55]. We put the accent on substoichiometric niobium nitride δ-$NbN_{0.875}$ (or B1-$NbN_{0.875}$) that was mixed with stoichiometric cubic aluminium nitride, B1-AlN. The motivation was the fact that stoichiometric cubic niobium nitride is dynamically unstable, for which reason it cannot be synthesized without nitrogen vacancies [56,57]. First-principles calculations were carried out using the Quantum-ESPRESSO code [58]. Vanderbilt ultra-soft pseudo-potentials were used to describe the electron-ion interaction [59]. The semi-core states were treated as valence states. The generalized gradient approximation (GGA) of Perdew *et al.* [60] was employed to describe exchange-correlation energy. The criterion of convergence for the total energy was 10^{-6} Ry/cell. To speed up convergence, each eigenvalue was convoluted with a Gaussian with a width of 0.03 Ry (0.408 eV). The cut-off energy for the plane-wave basis was set to 38 Ry (516.8 eV). The integration in the Brillouin zone (BZ) was done on special **k**-points determined according to the Monkhorst-Pack scheme using a non-shifted mesh (4 2 2). All initial structures were optimized by simultaneously relaxing the supercell basis vectors and the atomic positions inside the supercells using the Broyden–Fletcher–Goldfarb–Shanno (BFGS) algorithm [61]. The relaxation of the initial

structures was considered to be complete when atomic forces were less than 1.0 mRy/Bohr (25.7 meV/Å), stresses were smaller than 0.05 GPa, and the total energy during the structural optimization iterative process was changing by less than 0.1 mRy (1.36 meV). The phonon spectra of the alloys were calculated using the PHONOPY code [62]. The Gibbs free energy of mixing, G_{mix}, is given by:

$$G_{mix}(x,T) = G(Nb_{1-x}Al_xN_{(7+x)/8}) - (1-x)\cdot G(NbN_{0.875}) - x\cdot G(AlN),$$

where each G value contains electronic, configurational and vibrational (phonon) terms [63]. The vibrational contribution was calculated neglecting anaharmonic effects.

Results and Discussion

Experimental results

The elemental composition of the deposited films is presented in the Table 2 as a function of the current I_{Al}. It is obvious that the Al concentration increases with increasing the current at the Al target. At the same time, the concentration of oxygen decreases due to increasing in film densification and changing a structure type.

Figures 1a– 1c show the AFM surface topography of the as-deposited and annealed at T_{an} = 1000°C films. Weakly columnar structure is observed. The surface roughness slightly increases with T_{an}, see Fig. 1d. On the contrary, it decreases from 4.82 nm to 1.61 nm with increasing the current I_{Al}.

The observed reduction of surface roughness can be explained by decreasing grain size due to appearing a large amount of atoms after adding a doping element [64]. In addition, surface diffusion leads to smoothing the surface of the coating [65,66]. The surface roughness increased to 2.66 nm after annealing, which can be explained by the formation of faceted phases of oxides with good crystallization [67]. The smallest values of the surface roughness of the sample 5 can be explained by the formation of the amorphous phase in the nanocrystalline structure of the coating.

In Figure 2 we show the XRD patterns of the Nb-Al-N coatings, before and after annealing. An asymmetric shift of peaks towards large angles can be seen. Separation of these peaks showed, that two phases appeared during deposition: δ-NbN_x (marked by arrows) and δ-(Nb,Al)N phases that formed a solid solution.

We calculated concentration of Al in the first and second phases using Vegard's rule [68], it was less than 4 at.% and less than 14 at.% accordingly. We used a(AlN) = 4.069 Å for samples 2 – 6, and a(NbN)=4.376 Å for Sample 1 [69] as reference values. Structural characteristics of the coatings under investigation are presented in the Table 2.

An application of high currents (250, 300 mA – Samples 5 and 6) to the Al target (curve 1 in Fig. 2a and curve 3 in Fig. 2b) led to appearing halo-like component in the range of angles 18 – 30°, which confirmed the existence of the amorphous phase in the coating. Changes of this component after annealing (see curve 2 in Fig. 2a) indicates recrystallization of the coating due to annealing and decreasing amorphous phase. The preferred plane of growth remains (200) after annealing, but crystallites with the (400) orientation disappear, and (311) oriented crystallites appear. The size of the crystallites of the δ-NbN_x phase increased 1.6÷1.9 times as compared to those of as-deposited samples. By the way, we did not observe changes in the size of the grains in δ-(Nb,Al)N phase, and the as-deposited coating had more ordered structure in comparison with annealed one (sample 1, curve 3 in the Fig. 2a).

Ordering of the coating structure growth was observed in the sample with small content of Al in the as-deposited state (curve 3 in the Fig. 2a) and in the sample with high content of Al (curve 3 in the Fig. 2a). These findings differ from the results for Sample 1 (curve 1 in the Fig. 2a). A formation of the preferred orientation (200) caused the reduction of the coating surface energy [70,71].

Figure 3 shows the SEM image of the Nb-Al-N coatings before (a-c) and after annealing (d). Strong columnar structure is observed only for Sample 1, in agreement with the AFM observations (see Fig. 1a). The surface of the coatings is almost smooth for other samples. There are no significant changes in the surface roughness after annealing, thus we can conclude, that thermal stability of the coatings is quite high [72].

In Figure 4 we present the TEM image of the cross-section of the sample 6. We can see columnar structure of the coating growth. Studies of the transition layer between the coating and substrate (Fig. 5) detected a thin 3.6 nm layer of silicon

oxide that was deposited due to short-time reactive sputtering of oxygen before coating deposition in order to form diffusion barrier between substrate and coating. Grains were not detected near the surface of the oxidized layer. Fast Fourier Transformation (FFT) method [73] was applied to this layer and we did not found any peaks, which confirmed the absence of any periodical structure in this layer.

FFT studies of the surface of the coatings (Fig. 6a) showed three different structural components (Fig. 6b). Reverse FFT images of each structure are presented in Figs. 6c, 6d and 6e, respectively. An inspection of the red and green regions indicates the presence of 3÷4 nm nanoparticles, which is consistent with the results of XRD studies of the size of grains in the δ-NbN_x phase (see Table 1). Based on TEM results we can assume, that δ-(Nb,Al)N solid solution was not formed in the near-surface regions, despite the fact that Musil [74] suggested that such phases could appear in the near-surface regions and this could be the reason for low roughness of the coatings. The nc-NbN/a-AlN nanocomposite structure near the coating surface forms a protective layer against oxidation. This is confirmed by decreasing the oxygen concentration in the samples 5 and 6 compared to that in the samples 1 and 2 that consist only of the δ-NbN_x or δ-(Nb,Al)N phase (cf. Table 2). At the same time, δ-NbN_x and δ-(Nb,Al)N phases (probably, embedded into the a-AlN matrix) form in the depth of the coatings.

Figure 7 shows the diffraction patterns of the sample 6 combined with corresponding light-field images and SAED pattern. One can see that the fcc lattice was formed in the coating (see Fig. 7c and 7g). Preferred orientation of the crystal planes was not observed. SAED patterns (Fig. 7d) points to the formation of four crystallographic orientations, such as (200), (220), (311) and (400), which is consistent with the results [9].

Distribution of the coating elements over the depth determined by EDX is presented. The thickness of the coating is 1.16 μm, The Nb concentration decreased with increasing coating thickness.

Dependencies of hardness, elastic modulus and wear on Al concentration are presented in Fig. 9. Doping of Al into the coating led to decreasing hardness and elastic modulus from 27 GPa to 19.5 GPa and from 300 GPa to 190 GPa,

respectively. However, wear resistance of the coatings increased. It is characterized by H/E ratio [75,76] that was in the range from 0.09 to 0.1. Mechanical properties of the coatings did not change after annealing at the temperature 1000 ^{o}C, which indicates high thermal stability of the deposited coatings. Thus, we can assume that the deposited Nb-Al-N coatings are perspective as wear-resistant ones.

Theoretical results

In Fig. 10 we show the lattice parameter (a) after structural optimization as a function of composition. We note that the lattice constant shows a positive deviation from Vegard's law (dashed line). This fact usually indicates towards phase separation.

The Gibbs free energy of mixing for B1-$Nb_{1-x}Al_xN_{(7+x)/8}$ random alloy, calculated at different temperatures, are presented in Fig. 11 as a function of the fraction of AlN, x. The positive formation energy implies that the alloys are not stable, and will decompose into $NbN_{0.875}$ and AlN with the chemical driving force (G_{mix}). However, the alloys can be stabilized in some range of composition depending on temperature, owing to configurational and vibrational contributions. Figure 11 shows also that the vibrational contribution strongly reduces the Gibbs free energy of mixing at high temperatures.

In Figure 12 we compare the phase diagram with that calculated neglecting lattice vibrations. The difference in both the calculated phase diagrams is dramatic. By allowing for the phonon contribution, the maximum of the miscibility gap reduces from 11000 K to 6000 K. We see that, for small Al fractions, x, the solid solutions will form in agreement with our experimental results. At moderate temperatures (less than 1000 K), when diffusion will activated, a further increase in x will lead to phase segregation thorough spinodal decomposition. We assume that it is the spinodal decomposition of Nb-Al-N solid solutions that is responsible for the formation of the observed nanocomosite structure of the deposited Nb-Al-N films.

Conclusions

Nb-Al-N coatings were deposited using magnetron sputtering on silicon substrates. An application of different currents in the range 0÷300 mA to the Al target led to different concentrations of Al in the coatings.

Phase transformations were observed in the coatings depending on the current supplied to the Al target (I_{Al}). First, the δ-NbN_x phase and then solid solutions δ-$(Nb,Al)N_x$ formed in the coatings deposited at I_{Al} = 0÷50 mA. The nanocomposite structure that consisted of the mixture of δ-NbN_x and δ-$(Nb,Al)N_x$ phases was formed in the coatings deposited at I_{Al} = 100÷150 mA. At I_{Al} = 250÷300 mA, the nc-NbN/a−AlN nanocomposite structure forms on and near the coating surface, and the nc-NbN_x/nc-$(Nb,Al)N_x$/a-AlN structure was observed in the middle of the coatings. The formation of different phases was caused by an inhomogeneous distribution of elements over the depth of the coatings. As the result, the roughness of the coatings decreased with increasing the Al concentration due to decreasing grain size. Annealing did not lead to changes in surface roughness, grain size and mechanical properties of the coatings. Comparatively high values of H/E ratios make the coating suitable for the use as wear-resistant coatings.

First-principles investigation of Nb-Al-N solid solutions was carried out to interpret film properties. In particular, the phase diagram for solid solutions was calculated. It was show an important role of the phonon contribution to the Gibbs free energy of mixing. By allowing for the phonon contribution, the maximum of the miscibility gap reduces from 11000 K to 6000 K. The calculated phase diagram shows that for small Al fractions, x, the solid solutions will form in agreement with our experimental results. A further increase in x will lead to phase segregation thorough spinodal decomposition. The spinodal decomposition of Nb-Al-N solid solutions is supposed to be responsible for the formation of the nanocomosite structure observed in the deposited Nb-Al-N films.

Acknowledgements

This work was done under the aegis of Ukrainian state budget programs: “Development of material science fundamentals of structure engineering of vacuum-

plasma superhard coatings with given functional properties" (registration number 0115U000682), "Physical basics of forming of composition and properties of transition metals boride, nitride and boride-nitride films to be used in machine-building" (registration number 0116U002621) and "Development of perspective nanostructured multilayered coatings with enhanced physical-mechanical and tribological properties" (registration number 0116U006816).

References

[1] M. Hajenius, J.J.A. Baselmans, J.R. Gao, T.M. Klapwijk, P.A.J. de Korte, B. Voronov, G. Gol'tsman, Low noise NbN superconducting hot electron bolometer mixers at 1.9 and 2.5 THz, Supercond. Sci. Technol. 17 (2004) S224–S228. doi:Doi 10.1088/0953-2048/17/5/026\nPii S0953-2048(04)72773-6.

[2] L. Kang, B.B. Jin, X.Y. Liu, X.Q. Jia, J. Chen, Z.M. Ji, W.W. Xu, P.H. Wu, S.B. Mi, A. Pimenov, Y.J. Wu, B.G. Wang, Suppression of superconductivity in epitaxial NbN ultrathin films, J. Appl. Phys. 109 (2011) 2–7. doi:10.1063/1.3518037.

[3] S. Thakoor, H.G. LeDuc, A.P. Thakoor, J. Lambe, S.K. Khanna, Room temperature deposition of superconducting NbN for superconductor--insulator--superconductor junctions, J. Vac. Sci. Technol. A. 4 (1986) 528–531. doi:10.1116/1.573873.

[4] J. Kitaygorsky, I. Komissarov, A. Jukna, D. Pan, O. Minaeva, N. Kaurova, A. Divochiy, A. Korneev, M. Tarkhov, B. Voronov, I. Milostnaya, G. Gol'tsman, R.R. Sobolewski, Dark Counts in Nanostructured NbN Superconducting Single-Photon Detectors and Bridges, IEEE Trans. Appl. Supercond. 17 (2007) 275–278. doi:10.1109/TASC.2007.898109.

[5] K. Suzuki, S. Miki, S. Shiki, Z. Wang, M. Ohkubo, Time Resolution Improvement of Superconducting NbN Stripline Detectors for Time-of-Flight Mass Spectrometry, Appl. Phys. Express. 1 (2008) 031702. doi:10.1143/APEX.1.031702.

[6] A.D. Pogrebnjak, D. Eyidi, G. Abadias, O.V. Bondar, V.M. Beresnev, O.V. Sobol, Structure and properties of arc evaporated nanoscale TiN/MoN multilayered systems, Int. J. Refract. Met. Hard Mater. 48 (2015) 222–228. doi:10.1016/j.ijrmhm.2014.07.043.

[7] V.I. Ivashchenko, P.L. Skrynskii, O.S. Litvin, A.D. Pogrebnjak, V.N. Rogoz, G. Abadias, O. V. Sobol', A.P. Kuz'menko, Structure and properties of nanostructured NbN and Nb-Si-N films depending on the conditions of deposition: Experiment and theory, Phys. Met. Metallogr. 116 (2015) 1015–1028. doi:10.1134/S0031918X15080062.

[8] V.I. Ivashchenko, P.L. Scrynskyy, O.S. Lytvyn, V.M. Rogoz, O. V. Sobol, A.P. Kuzmenko, H. Comsta, C. Karvat, Investigation of NbN and Nb-Si-N Coatings Deposited by Magnetron Sputtering, ACTA Phys. Pol. A. 128 (2015) 949–952. http://apps.webofknowledge.com/full_record.do?product=UA&search_mode=GeneralSearch&qid=19&SID=R1bL9S9LnrDYnz2OxSD&page=1&doc=1 (accessed January 27, 2016).

[9] A.D. Pogrebnjak, O. V. Bondar, G. Abadias, V. Ivashchenko, O. V. Sobol, S. Jurga, E. Coy, Structural and mechanical properties of NbN and Nb-Si-N films: Experiment and molecular dynamics simulations, Ceram. Int. 42 (2016) 11743–11756. doi:10.1016/j.ceramint.2016.04.095.

[10] J.C. Villegier, L. Vieux-Rochaz, M. Goniche, P. Renard, Vabre M., NbN tunnel junctions, IEEE Trans. Magn. MAG-21 (1985) 498–504.

[11] M. Aoyagi, S. Kosaka, A. Shoji, F. Shinoki, S. Tahara, An integration of all refractory josephson logic LSI circuit, IEEE Trans. Magn. 3 (1980) 451–453. doi:10.1111/j.1365-2761.1980.tb00431.x.

[12] A. Shoji, M. Aoyagi, S. Kosaka, F. Shinoki, Temperature-dependent properties of niobium nitride josephson tunnel junctions, IEEE Trans. Magn. 23 (1987) 1464–1471.

doi:10.1109/TMAG.1987.1064829.
[13] H. Leduc, All refractory NbN/MgO/NbN tunnel junctions, IEEE Trans. Magn. Mag-23 (1987) 863–865. doi:10.1017/CBO9781107415324.004.
[14] M. Leung, U. Strom, J.C. Culbertson, J.H. Claassen, S.A. Wolf, R.W. Simon, NbN/BN granular films - a novel broadband bolometric detector for pulsed far infrared radiation, IEEE Trans. Magn. 23 (1987) 714–716.
[15] S.A. Wolf, U. Strom, J.C. Culbertson, D. Paget, Superconducting granular NbN bolometer ultrafast for spectroscopy, IEEE Trans. Magn. 21 (1985) 920–923.
[16] Y.B. Vachtomin, M. Finkel, S. V Antipov, B.M. Voronov, V. Smimov, N.S. Kaurova, V.N. Drakinski, G.N. Gortsman, Gain bandwidth of phonon-cooled HEB mixer made of NbN thin film with MgO buffer layer on Si, in: Thirteen. Int. Symp. Sp. Temhertz Technol. Harvard Univ., 2002.
[17] P. Khosropanah, J.R. Gao, W.M. Laauwen, M. Hajenius, T.M. Klapwijk, Low noise NbN hot electron bolometer mixer at 4.3 THz, Appl. Phys. Lett. 91 (2007) 1–3. doi:10.1063/1.2819534.
[18] J.W. Kooi, J.J.A. Baselmans, M. Hajenius, J.R. Gao, T.M. Klapwijk, P. Dieleman, A. Baryshev, G. de Lange, IF impedance and mixer gain of NbN hot electron bolometers, J. Appl. Phys. 101 (2007) 1–8. doi:10.1063/1.2400086.
[19] A. Korneev, A. Lipatov, O. Okunev, G. Chulkova, K. Smirnov, G. Gol'tsman, J. Zhang, W. Slysz, A. Verevkin, R. Sobolewski, GHz counting rate NbN single-photon detector for IR diagnostics of VLSI CMOS circuits, Microel. Eng. 69 (2003) 274–278. doi:10.1016/S0167-9317(03)00309-5.
[20] K. Senapati, N. Pandey, R. Nagar, R. Budhani, Normal-state transport and vortex dynamics in thin films of two structural polymorphs of superconducting NbN, Phys. Rev. B. 74 (2006) 1–8. doi:10.1103/PhysRevB.74.104514.
[21] W. Słysz, M. Węgrzecki, J. Bar, P. Grabiec, M. Górska, V. Zwiller, C. Latta, P. Bohi, I. Milostnaya, O. Minaeva, A. Antipov, O. Okunev, A. Korneev, K. Smirnov, B. Voronov, N. Kaurova, G. Gol'tsman, A. Pearlman, A. Cross, I. Komissarov, A. Verevkin, R. Sobolewski, Fiber-coupled single-photon detectors based on NbN superconducting nanostructures for practical quantum cryptography and photon-correlation studies, Appl. Phys. Lett. 88 (2006) 1–3. doi:10.1063/1.2218105.
[22] J. Zhang, W. Slysz, A. Verevkin, O. Okunev, G. Chulkova, A. Korneev, A. Lipatov, G.N. Gol'tsman, R. Sobolewski, Response time characterization of NbN superconducting single-photon detectors, IEEE Trans. Appl. Supercond. 13 (2003) 180–183. doi:10.1109/TASC.2003.813675.
[23] G.N. Gol'tsman, O. Okunev, G. Chulkova, A. Lipatov, A. Semenov, K. Smirnov, B. Voronov, A. Dzardanov, C. Williams, R. Sobolewski, Picosecond superconducting single-photon optical detector, Appl. Phys. Lett. 79 (2001) 705–707. doi:10.1063/1.1388868.
[24] J. Kitaygorsky, J. Zhang, A. Verevkin, A. Sergeev, A. Korneev, V. Matvienko, P. Kouminov, K. Smirnov, B. Voronov, G. Gol'tsman, R. Sobolewski, Origin of Dark Counts in Nanostructured NbN Single-Photon Detectors, IEEE Trans. Appiled Supercond. 15 (2005) 545–548. doi:10.1109/TASC.2005.849914.
[25] T.N. Koltunowicz, P. Zukowski, V. Bondariev, K. Czarnacka, O. Boiko, J.A. Fedotova, J.V. Kasiuk, Study of dielectric function of (FeCoZr)x(CaF2)(100-x) nanocomposites produced with a beam of argon ions, J. Alloys Compd. 650 (2015) 262–267. doi:10.1016/j.jallcom.2015.07.276.
[26] J.V. Kasiuk, J.A. Fedotova, T.N. Koltunowicz, P. Zukowski, A.M. Saad, J. Przewoznik, C. Kapusta, J. Zukrowski, I.A. Svito, Correlation between local Fe states and magnetoresistivity in granular films containing FeCoZr nanoparticles embedded into oxygen-free dielectric matrix, J. Alloys Compd. 586 (2014) S432–S435. doi:10.1016/j.jallcom.2012.09.058.
[27] I. Svito, J.A. Fedotova, M. Milosavljević, P. Zhukowski, T.N. Koltunowicz, A. Saad, K. Kierczynski, A.K. Fedotov, Influence of sputtering atmosphere on hopping conductance in granular nanocomposite (FeCoZr)x(Al2O3)1- x films, J. Alloys Compd. 615 (2014) S344–S347. doi:10.1016/j.jallcom.2013.12.061.

[28] A.D. Pogrebnjak, G. Abadias, O. V. Bondar, O. V. Sobol, V.M. Beresnev, A. V. Pshyk, A.A. Demianenko, K.O. Belovol, D.A. Kolesnikov, H. Komsta, High temperature annealing of ion-plasma nanostructured coatings based on AlN-TiB2(TiSi2), Acta Phys. Pol. A. 125 (2014) 1284–1287. doi:10.12693/APhysPolA.125.1284.

[29] P. Zukowski, T.N. Koltunowicz, O. Boiko, V. Bondariev, K. Czarnacka, J.A. Fedotova, A.K. Fedotov, I.A. Svito, Impedance model of metal-dielectric nanocomposites produced by ion-beam sputtering in vacuum conditions and its experimental verification for thin films of (FeCoZr)x(PZT)(100-x), Vacuum. 120 (2015) 37–43. doi:10.1016/j.vacuum.2015.04.035.

[30] A. Shypylenko, A.V. Pshyk, B. Grześkowiak, K. Medjanik, B. Peplinska, K. Oyoshi, A. Pogrebnjak, S. Jurga, E. Coy, Effect of ion implantation on the physical and mechanical properties of Ti-Si-N multifunctional coatings for biomedical applications, Mater. Des. 110 (2016) 821–829. doi:10.1016/j.matdes.2016.08.050.

[31] A.D. Pogrebnjak, Structure and Properties of Nanostructured (Ti-Hf-Zr-V-Nb)N Coatings, J. Nanomater. 2013 (2013) 1–12. doi:10.1155/2013/780125.

[32] A.D. Pogrebnjak, A.G. Ponomarev, A.P. Shpak, Y.A. Kunitskii, Application of micro- and nanoprobes to the analysis of small-sized 3D materials, nanosystems, and nanoobjects, Phys. Usp. 182 (2012) 287–321. doi:10.3367/UFNr.0182.201203d.0287.

[33] H. Barshilia, N. Selvakumar, B. Deepthi, A comparative study of reactive direct current magnetron sputtered CrAlN and CrN coatings, Surf. Coatings. 201 (2006) 2193–2201. http://sci-hub.cc/http://www.sciencedirect.com/science/article/pii/S0257897206002702 (accessed July 29, 2016).

[34] X.-Z. Ding, X.T. Zeng, Structural, mechanical and tribological properties of CrAlN coatings deposited by reactive unbalanced magnetron sputtering, Surf. Coatings Technol. 200 (2005) 1372–1376. doi:DOI 10.1016/j.surfcoat.2005.08.072.

[35] R. Wuhrer, W.Y. Yeung, A comparative study of magnetron co-sputtered nanocrystalline titanium aluminium and chromium aluminium nitride coatings, Scr. Mater. 50 (2004) 1461–1466. doi:10.1016/j.scriptamat.2004.03.007.

[36] A. Höling, L. Hultman, M. Odén, J. Sjölén, L. Karlsson, Mechanical properties and machining performance of Ti1-xAlxN-coated cutting tools, Surf. Coatings Technol. 191 (2005) 384–392. doi:10.1016/j.surfcoat.2004.04.056.

[37] O. Knotek, On structure and properties of sputtered Ti and Al based hard compound films, J. Vac. Sci. Technol. A. 4 (1986) 2695–2700. doi:10.1116/1.573708.

[38] W.-D. Münz, Titanium aluminum nitride films: A new alternative to TiN coatings, J. Vac. Sci. Technol. A Vacuum, Surfaces, Film. 4 (1986) 2717–2725. doi:10.1116/1.573713.

[39] Y.C. Chim, X.Z. Ding, X.T. Zeng, S. Zhang, Oxidation resistance of TiN, CrN, TiAlN and CrAlN coatings deposited by lateral rotating cathode arc, Thin Solid Films. 517 (2009) 4845–4849. doi:10.1016/j.tsf.2009.03.038.

[40] A.E. Reiter, V.H. Derflinger, B. Hanselmann, T. Bachmann, B. Sartory, Investigation of the properties of Al1-xCrxN coatings prepared by cathodic arc evaporation, Surf. Coatings Technol. 200 (2005) 2114–2122. doi:10.1016/j.surfcoat.2005.01.043.

[41] D. McIntyre, J.E. Greene, and W.D.M. G. Håkansson, J.E. Sundgren, Oxidation of metastable single-phase polycrystalline Ti 0.5Al0.5N films: Kinetics and mechanisms, J. Appl. Phys. 67 (1990) 1542–1553. doi:10.1063/1.345664.

[42] H. Hasegawa, T. Suzuki, Effects of second metal contents on microstructure and micro-hardness of ternary nitride films synthesized by cathodic arc method, Surf. Coatings Technol. 188-189 (2004) 234–240. doi:10.1016/j.surfcoat.2004.08.033.

[43] J. Lin, B. Mishra, J.J. Moore, W.D. Sproul, A study of the oxidation behavior of CrN and CrAlN thin films in air using DSC and TGA analyses, Surf. Coatings Technol. 202 (2008) 3272–3283. doi:10.1016/j.surfcoat.2007.11.037.

[44] A. Kimura, H. Hasegawa, K. Yamada, T. Suzuki, Effects of Al content on hardness, lattice parameter and microstructure of Ti1−xAlxN films, Surf. Coatings Technol. 120-121 (1999) 438–441. doi:10.1016/S0257-8972(99)00491-0.

[45] A.D. Pogrebnjak, A.P. Shpak, N.A. Azarenkov, V.M. Beresnev, Structures and properties of hard and superhard nanocomposite coatings, Physics- Uspекhi. 52 (2009) 29–54.

doi:10.3367/UFNr.0179.200901b.0035.
[46] A.D. Pogrebnjak, A.A. Bagdasaryan, I. V Yakushchenko, V.M. Beresnev, The structure and properties of high-entropy alloys and nitride coatings based on them, Russ. Chem. Rev. 83 (2014) 1027–1061. doi:10.1070/RCR4407.
[47] B.Y. Man, L. Guzman, A. Miotello, M. Adami, Microstructure, oxidation and H2-permeation resistance of TiAlN films deposited by DC magnetron sputtering technique, Surf. Coatings Technol. 180-181 (2004) 9–14. doi:10.1016/j.surfcoat.2003.10.021.
[48] F. Vaz, L. Rebouta, M. Andritschky, M.F. da Silva, J.C. Soares, Thermal oxidation of Ti1 − xAlxN coatings in air, J. Eur. Ceram. Soc. 17 (1997) 1971–1977. doi:10.1016/S0955-2219(97)00050-2.
[49] L. Chen, J. Paulitsch, Y. Du, P.H. Mayrhofer, Thermal stability and oxidation resistance of Ti-Al-N coatings, Surf. Coatings Technol. 206 (2012) 2954–2960. doi:10.1016/j.surfcoat.2011.12.028.
[50] T.I. Selinder, D.J. Miller, K.E. Gray, M.R. Sardela Jr., L. Hultman, Phase formation and microstructure of Nb1-xAlx alloy films grown on MgO (001) by reactive sputtering: a new ternary phase, Vacuum. 46 (1995) 1401–1406. doi:10.1016/0042-207X(95)00161-1.
[51] Y. Makino, Prediction of phase change in pseudobinary transition metal aluminum nitrides by band parameters method, Surf. Coatings Technol. 193 (2005) 185–191. doi:10.1016/j.surfcoat.2004.07.035.
[52] M. Benkahoul, Niobium nitride based thin films deposited by dc reactive magnetron sputtering : NbN, NbSiN and NbAlN, EPFL, Lausanne, 2005.
[53] Y. Makino, K. Saito, Y. Murakami, K. Asami, Phase Change of Zr-Al-N and Nb-Al-N Films Prepared by Magnetron Sputtering Method, Solid State Phenom. 127 (2007) 195–200. doi:10.4028/www.scientific.net/SSP.127.195.
[54] J. Nieto, J. Caicedo, H. Moreno, W. Aperador, G. Bejarano, Influence of bias voltage on the corrosion resistance of Al-Nb-N thin films, Medellín. 77 (2010) 161–168.
[55] A. Zunger, S.-H. Wei, L.G. Ferreira, J.E. Bernard, Special quasirandom structures, Phys. Rev. Lett. 65 (1990) 353–356. doi:10.1016/j.commatsci.2014.09.021.
[56] W. Lengauer, M. Bohn, B. Wollein, K. Lisak, Phase Reaction in the Nb-N system below 1400 C, 48 (2000) 2633–2638.
[57] V.I. Ivashchenko, P.E.A. Turchi, E.I. Olifan, Phase stability and mechanical properties of niobium nitrides, Phys. Rev. B. 82 (2010) 054109. doi:10.1103/PhysRevB.82.054109.
[58] P. Giannozzi, S. Baroni, N. Bonini, M. Calandra, R. Car, C. Cavazzoni, D. Ceresoli, G.L. Chiarotti, M. Cococcioni, I. Dabo, A. Dal Corso, S. de Gironcoli, S. Fabris, G. Fratesi, R. Gebauer, U. Gerstmann, C. Gougoussis, A. Kokalj, M. Lazzeri, L. Martin-Samos, N. Marzari, F. Mauri, R. Mazzarello, S. Paolini, A. Pasquarello, L. Paulatto, C. Sbraccia, S. Scandolo, G. Sclauzero, A.P. Seitsonen, A. Smogunov, P. Umari, R.M. Wentzcovitch, QUANTUM ESPRESSO: a modular and open-source software project for quantum simulations of materials, J. Phys. Condens. Matter. 21 (2009) 395502. doi:10.1088/0953-8984/21/39/395502.
[59] D. Vanderbilt, Soft self-consistent pseudopotentials in a generalized eigenvalue formalism, Phys. Rev. B. 41 (1990) 7892–7895. doi:10.1103/PhysRevB.41.7892.
[60] J.P. Perdew, K. Burke, M. Ernzerhof, Generalized Gradient Approximation Made Simple, Phys. Rev. Lett. 77 (1996) 3865–3868. doi:10.1103/PhysRevLett.77.3865.
[61] S.R. Billeter, A. Curioni, W. Andreoni, Efficient linear scaling geometry optimization and transition-state search for direct wavefunction optimization schemes in density functional theory using a plane-wave basis, Comput. Mater. Sci. 27 (2003) 437–445. doi:10.1016/S0927-0256(03)00043-0.
[62] A. Togo, F. Oba, I. Tanaka, First-principles calculations of the ferroelastic transition between rutile-type and CaCl2-type SiO2 at high pressures, Phys. Rev. B - Condens. Matter Mater. Phys. 78 (2008) 1–9. doi:10.1103/PhysRevB.78.134106.
[63] C.K. Gan, Y.P. Feng, D.J. Srolovitz, First-principles calculation of the thermodynamics of InxGa1−xN alloys: Effect of lattice vibrations, Phys. Rev. B. 73 (2006) 235214. doi:10.1103/PhysRevB.73.235214.

[64] N. Jiang, Y.G. Shen, Y.-W. Mai, T. Chan, S.C. Tung, Nanocomposite Ti–Si–N films deposited by reactive unbalanced magnetron sputtering at room temperature, Mater. Sci. Eng. B. 106 (2004) 163–171. doi:10.1016/j.mseb.2003.09.033.
[65] G. Palasantzas, Roughness spectrum and surface width of self-afFine fractal surfaces via the K-correlation model, Phys. Rev. B. 48 (1993) 14472–14478. doi:10.1017/CBO9781107415324.004.
[66] S.K. Sinha, E.B. Sirota, S. Garoff, X-ray and neutron scattering from rough surfaces, Phys. Rev. B. 38 (1988) 2297–2311. doi:10.1103/PhysRevB.38.2297.
[67] M. Diserens, J. Patscheider, F. Lévy, Mechanical properties and oxidation resistance of nanocomposite TiN–SiNx physical-vapor-deposited thin films, Surf. Coatings Technol. 120-121 (1999) 158–165. doi:10.1016/S0257-8972(99)00481-8.
[68] L. Vegard, Die Konstitution der Mischkristalle und die Raumffillung der Atome, J. Mater. Sci. 1 (1921) 17–26. doi:10.1007/BF00549722.
[69] D. Holec, R. Franz, P.H. Mayrhofer, C. Mitterer, Structure and stability of phases within the NbN–AlN system, J. Phys. D. Appl. Phys. 43 (2010) 145403. doi:10.1088/0022-3727/43/14/145403.
[70] M. Wen, C.Q. Hu, C. Wang, T. An, Y.D. Su, Q.N. Meng, W.T. Zheng, Effects of substrate bias on the preferred orientation, phase transition and mechanical properties for NbN films grown by direct current reactive magnetron sputtering, J. Appl. Phys. 104 (2008) 1–7. doi:10.1063/1.2956706.
[71] C. V Thompson, Structure evolutionduring processing of polycrystalline films, Annu. Rev. Mater. Sci. 30 (2000) 159–190.
[72] J. Musil, Hard nanocomposite coatings: Thermal stability, oxidation resistance and toughness, Surf. Coatings Technol. 207 (2012) 50–65. doi:10.1016/j.surfcoat.2012.05.073.
[73] S. Kuo, B. Lee, Fast Fourier transform and its applications, in: Real Time Digit. Signal Process., 2001.
[74] J. Musil, Hard and superhard nanocomposite coatings, Surf. Coatings Technol. 125 (2000) 322–330. http://sci-hub.cc/http://www.sciencedirect.com/science/article/pii/S0257897299005861 (accessed August 1, 2016).
[75] L. Yate, L.E. Coy, G. Wang, M. Beltrán, E. Díaz-Barriga, E.M. Saucedo, M.A. Ceniceros, K. Zaleski, I. Llarena, M. Möller, R.F. Ziolo, Tailoring mechanical properties and electrical conductivity of flexible niobium carbide nanocomposite thin film, RSC Adv. 4 (2014) 61355–61362. doi:10.1039/c4ra11292j.
[76] E. Coy, L. Yate, Z. Kabacińska, M. Jancelewicz, S. Jurga, Topographic reconstruction and mechanical analysis of atomic layer deposited Al2O3/TiO2 nanolaminates by nanoindentation, Mater. Des. 111 (2016) 4–5. doi:10.1016/j.matdes.2016.09.030.

Table 1. Parameters of coating's deposition.

Sample	I_{Al}, mA	P_{Al}, W/cm^2	I_{Nb}, mA	P_{Nb}, W/cm^2	$P_{chamber}$, Pa
1	0	0	300	17.1	10^{-4}
2	50	2.9			
3	100	5.7			
4	150	8.6			

Table 2. EDX concentration of elements depending on the current at the Al target.

№	I_{Al}, mA	Nb	Al	N	O	Nb/Al
Sample 1	0	38.44	-	51.70	9.87	-
Sample 2	50	33.66	3.69	53.38	8.87	9.36
Sample 2 (Cross section)	50	24.52	3.43	62.22	9.83	7.15
Sample 4	150	37.91	5.37	50.48	6.26	7.06
Sample 5 (600C)	250	31.58	7.16	46.47	4.70	4.41
Sample 5 (800C)	250	37.88	6.86	49.85	5.41	5.52
Sample 5 (1000C)	250	31.50	8.83	53.53	6.13	3.57
Sample 6	300	22.77	18.40	53.11	5.71	1.24

Figures

Fig. 1. AFM images of Nb-Al-N coatings: sample 1 (a), sample 5 before (b) and after annealing (c). The surface rougness of the deposited films as a function of I_{Al}.(d)

Fig. 2. (a) XRD patterns of sample 5 before (curve 1) and after (curve 2) annealing in comparison with pattern for annealed Sample 1 (curve 3); (b) XRD patterns of sample 1 (curve 1), sample 4 (curve 2) and sample 6 (curve 3).

Fig. 3. SEM-images of Nb-Al-N coatings: Sample 1 (a), Sample 2 (b) and Sample 5 before (c) and after annealing (d).

Fig. 4. Light-field and dark-field TEM images of the cross-section of the Nb-Al-N coating (sample 6).

Fig. 5. TEM image of the transition layer between substrate and coating (sample 6) and their SAED patterns.

Fig. 6. TEM image of the surface of the Nb-Al-N coating (Sample 6)

Fig. 7. Diffraction patterns of sample 6 from the substrate (a), region between substrate and the coating (b) and from the coating (c), corresponding light-field images (e,f), SAED pattern (d), profile obtained along the blue line (g)

Fig. 8. Depth profile of the coating, obtained using EDX method (Sample 6).

Fig. 9. Hardness (H) (a), elasticity modulus (E) (b) and the H/E ratio (c) for the Sample 1 (black curve), Sample 4 (green curve) and Sample 5 after annealing (red curve).

Fig. 10. Lattice parameter (a) of $Nb_{1-x}Al_xN_{(7+x)/8}$ as a function of x. The dashed line is linear interpolation between the lattice parameters for $NbN_{0.875}$ and AlN.

Fig. 11. Gibbs free energy of mixing (G) for the alloys. The solid and dashed lines are G values calculated without and with phonon contribution, respectively.

Fig. 12. Calculated phase diagram for B1- $Nb_{1-x}Al_xN_{(7+x)/8}$ random alloy. The dashed and solid lines correspond to the bimodal (B) and spinodal (S) with and without vibrational contribution, respectively.

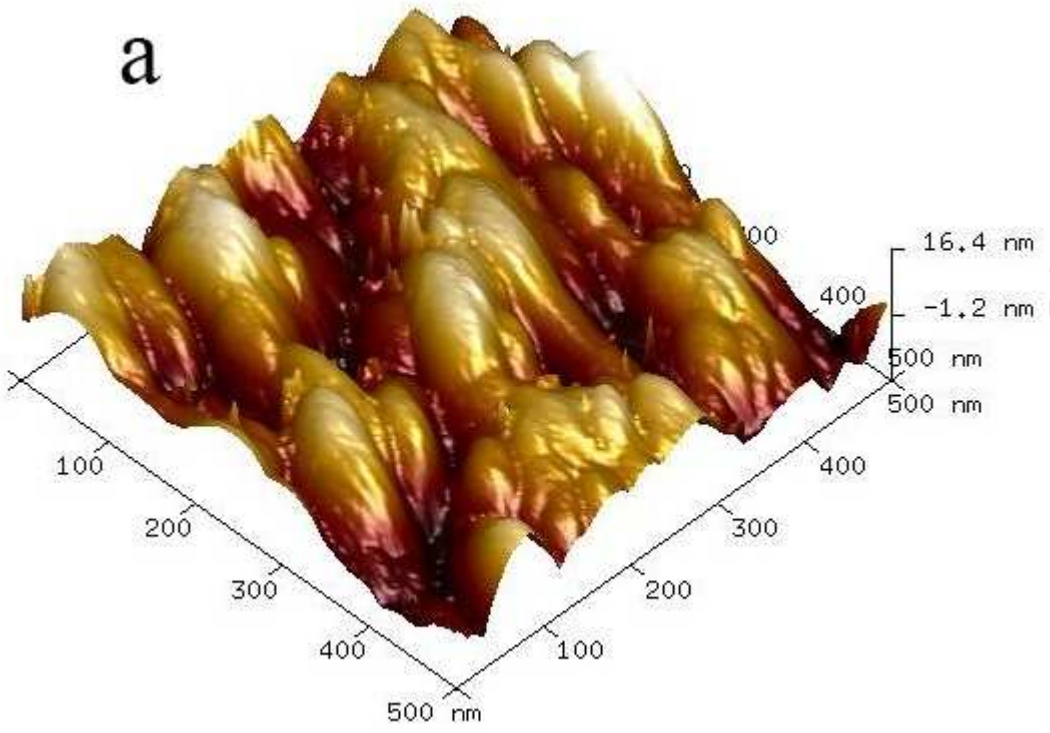

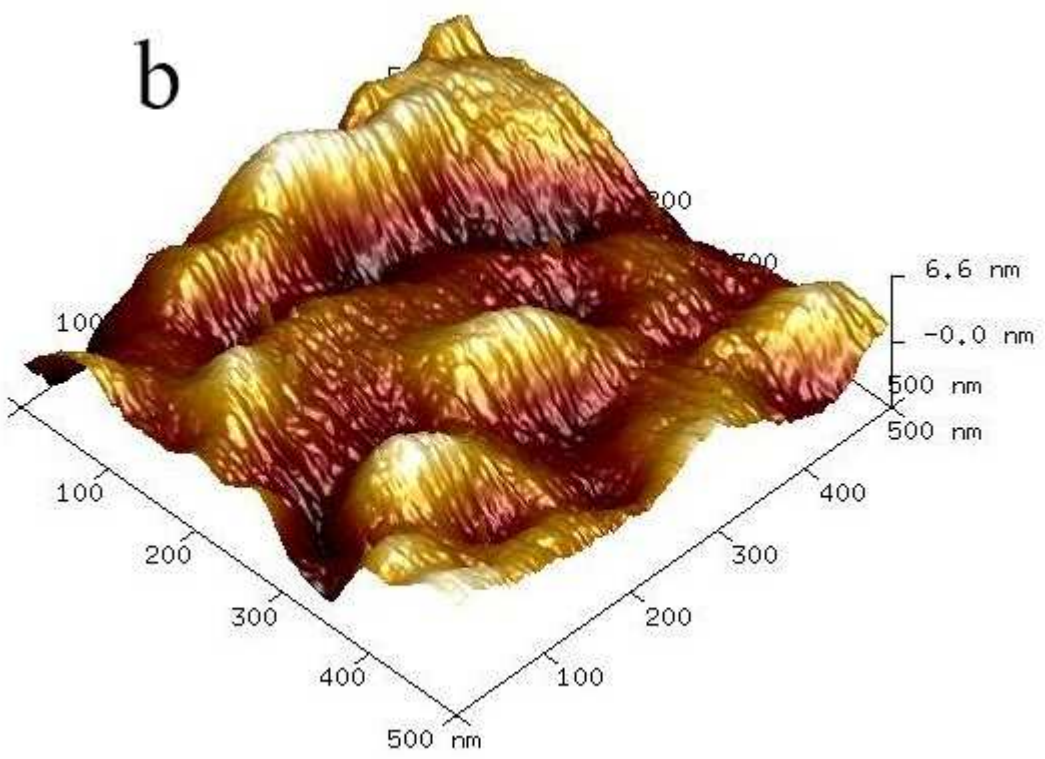

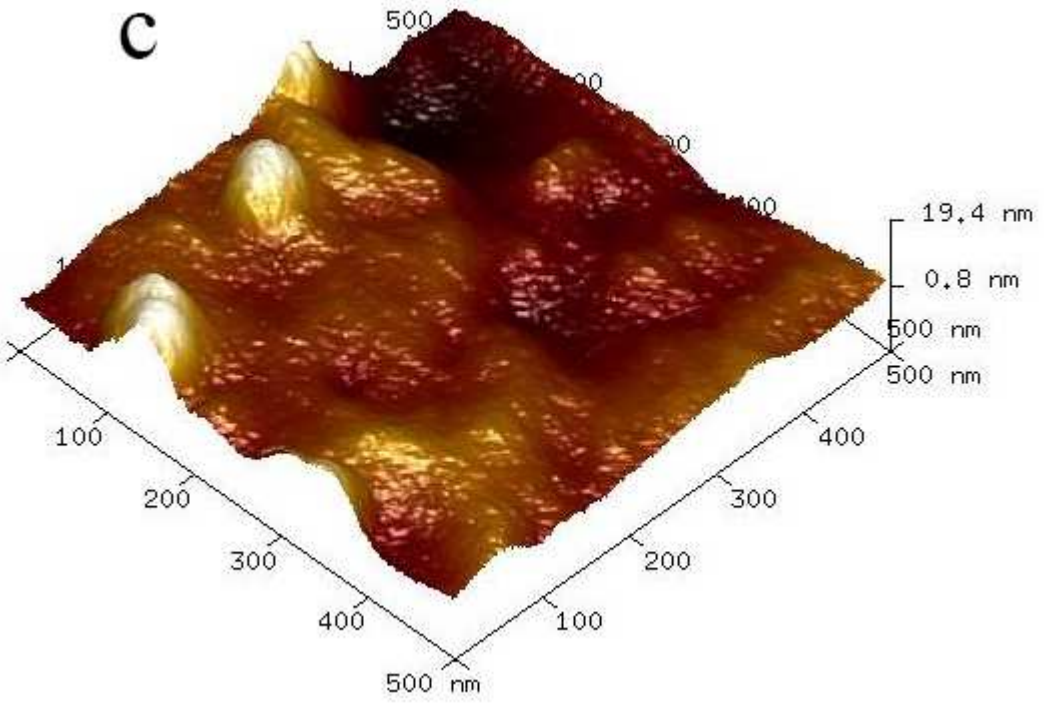

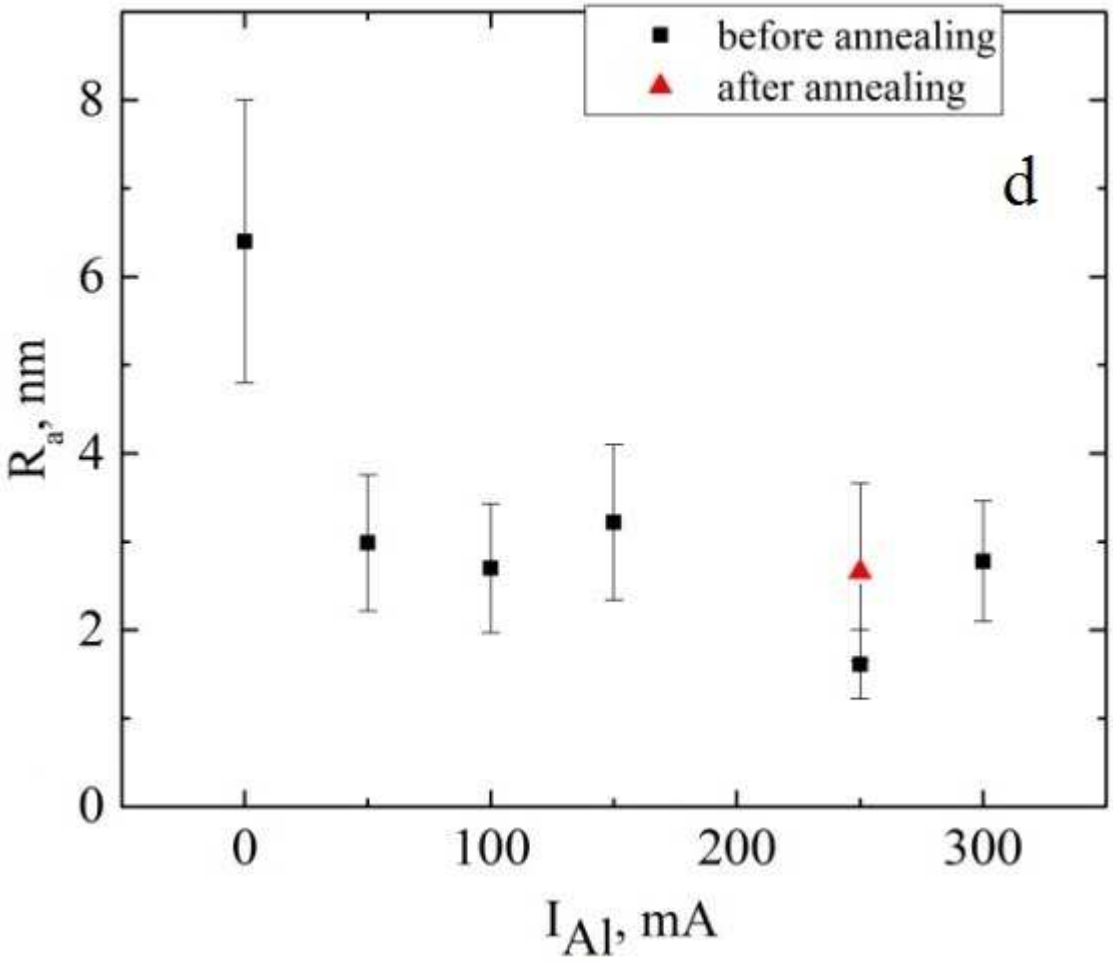
before annealing
after annealing
d
R_a, nm
0
2
4
6
8
0
100
200
300
I_{Al}, mA

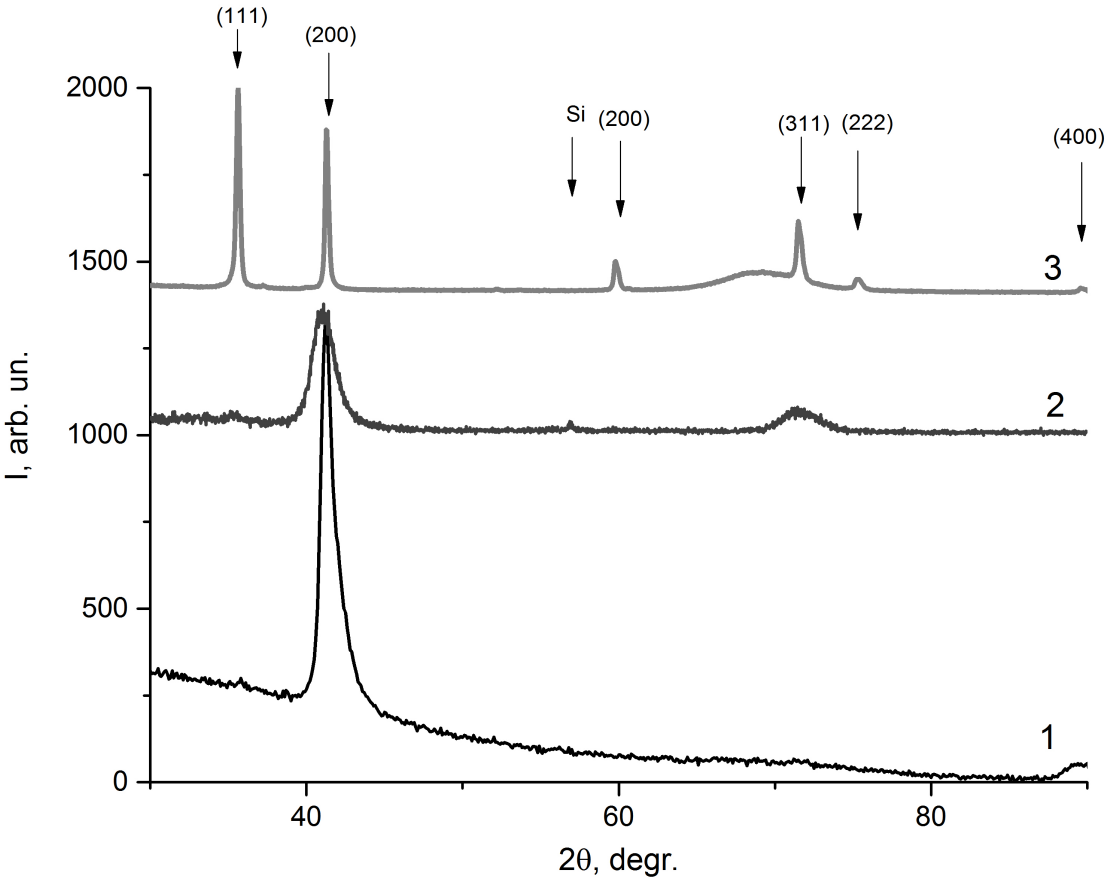

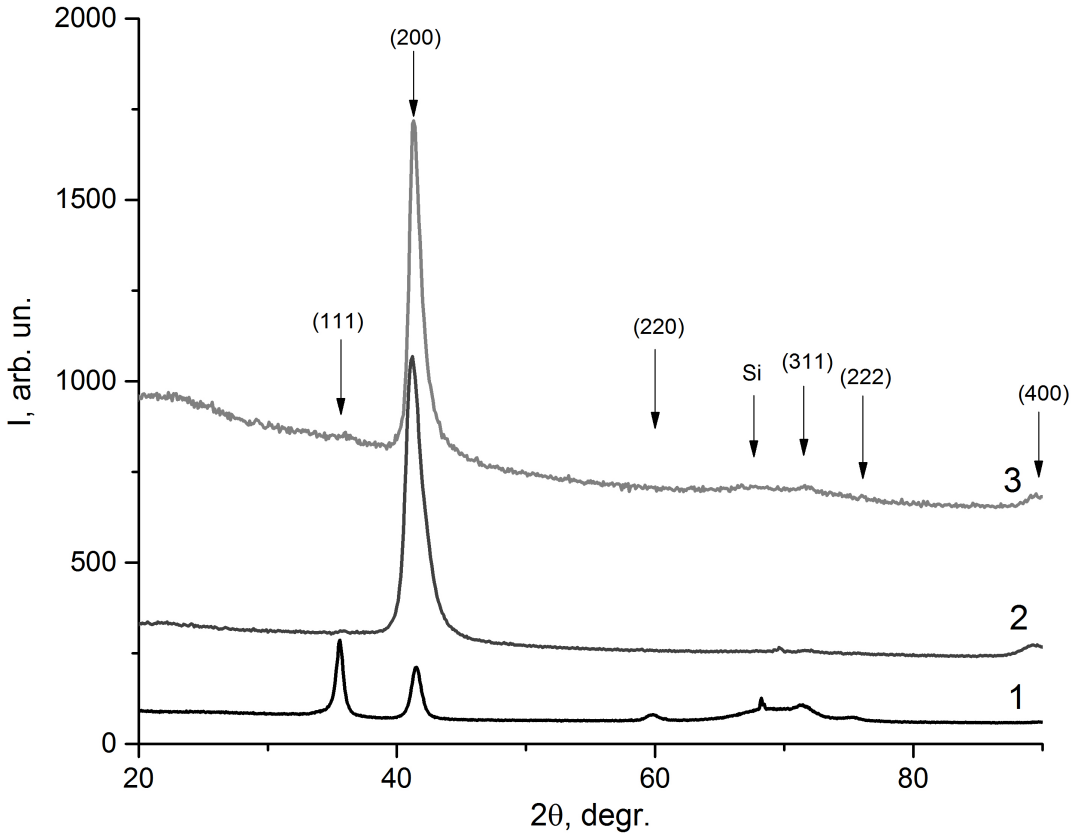

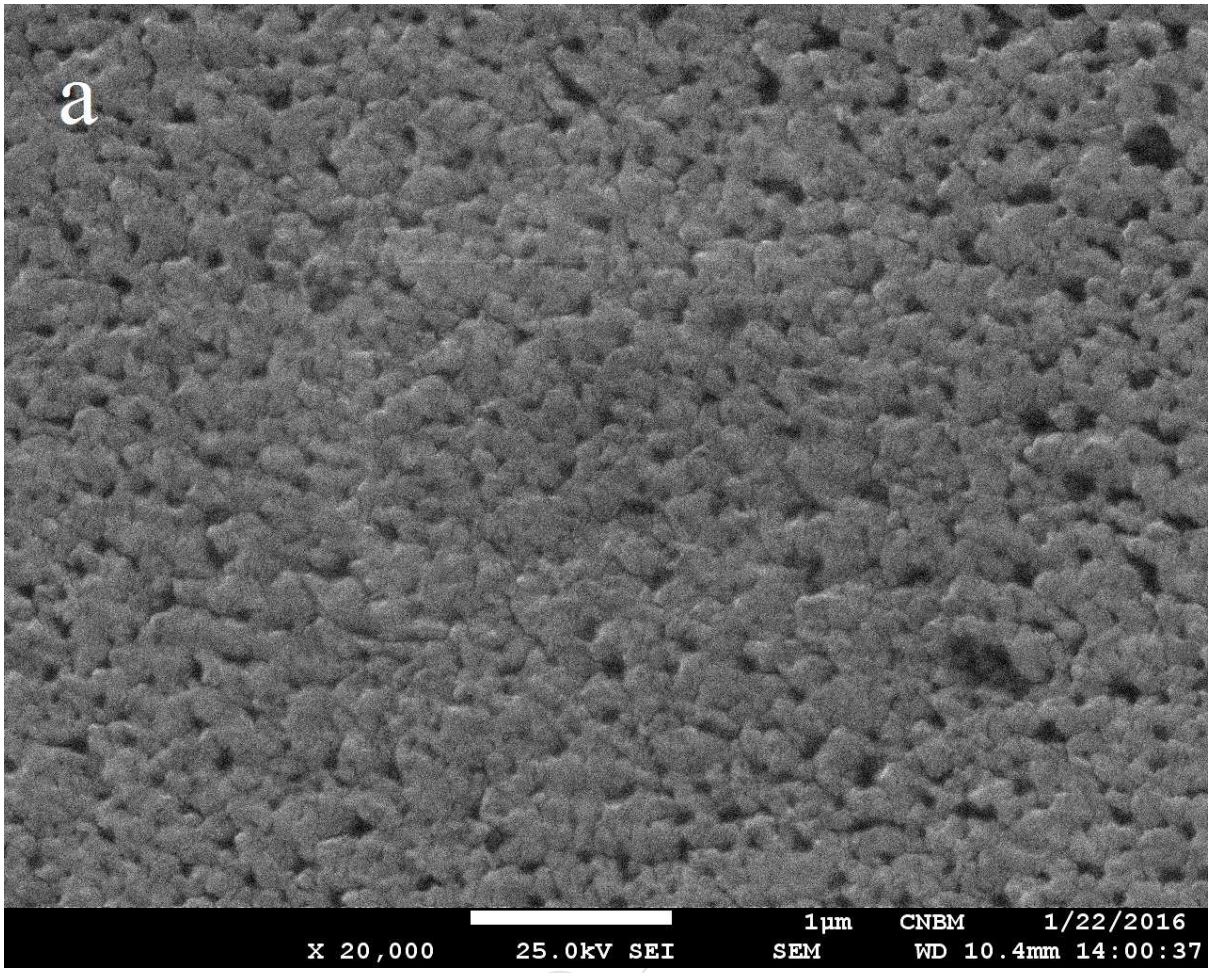

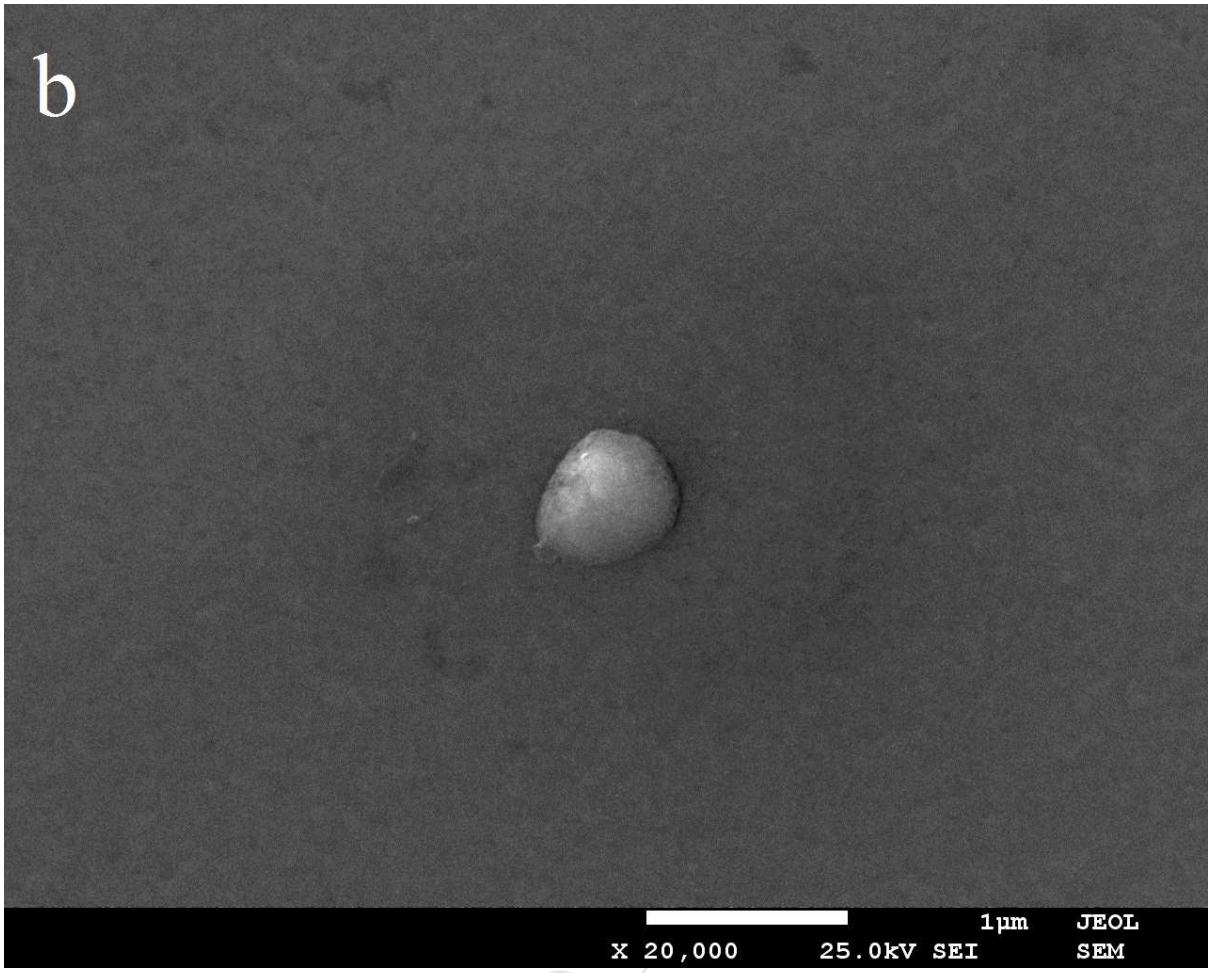

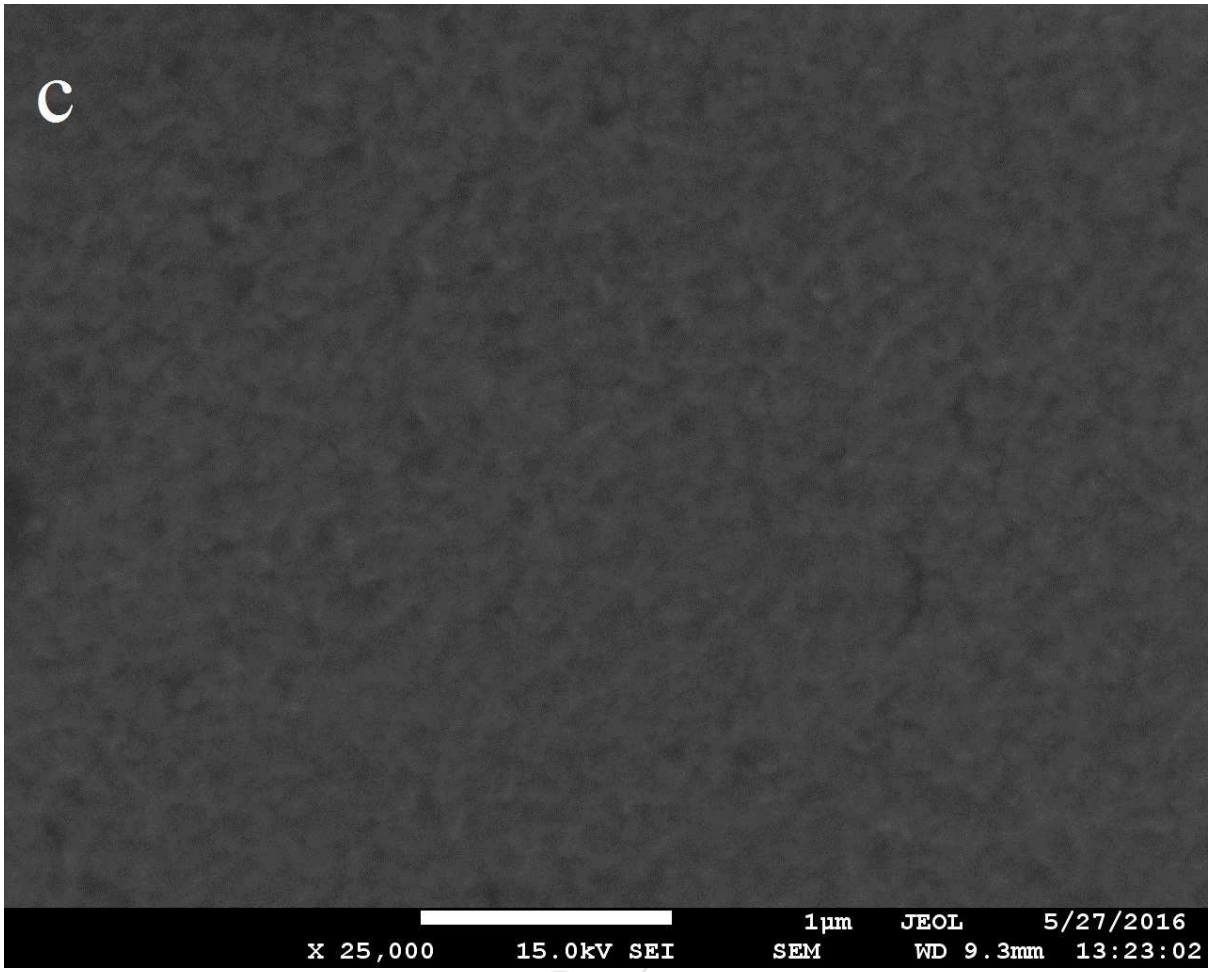

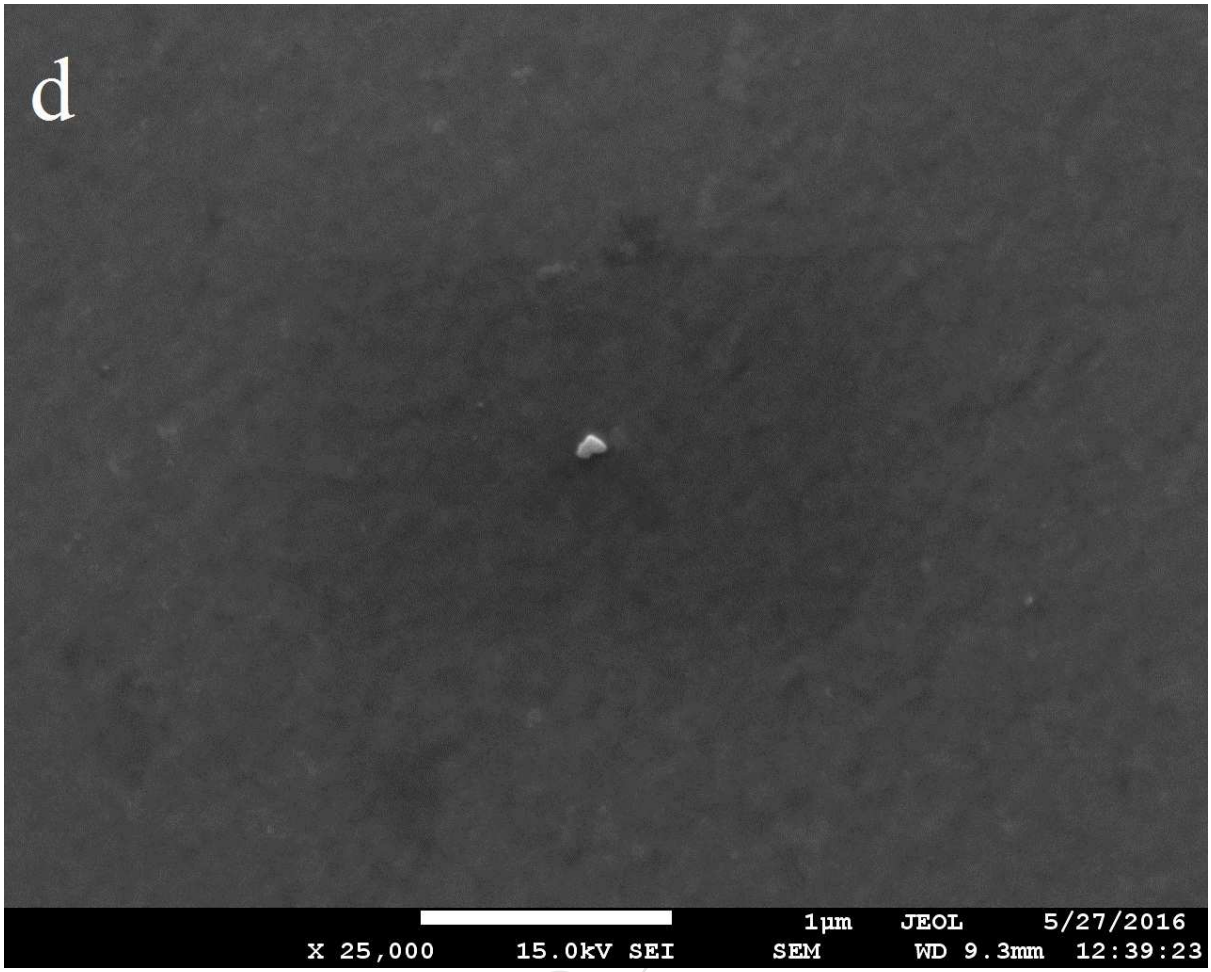

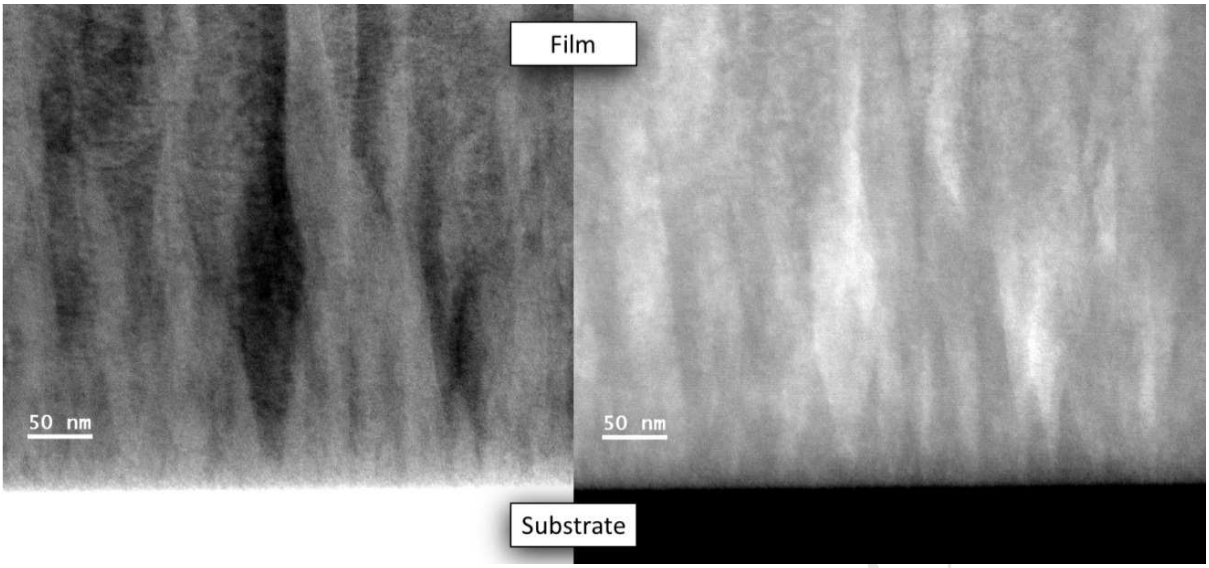

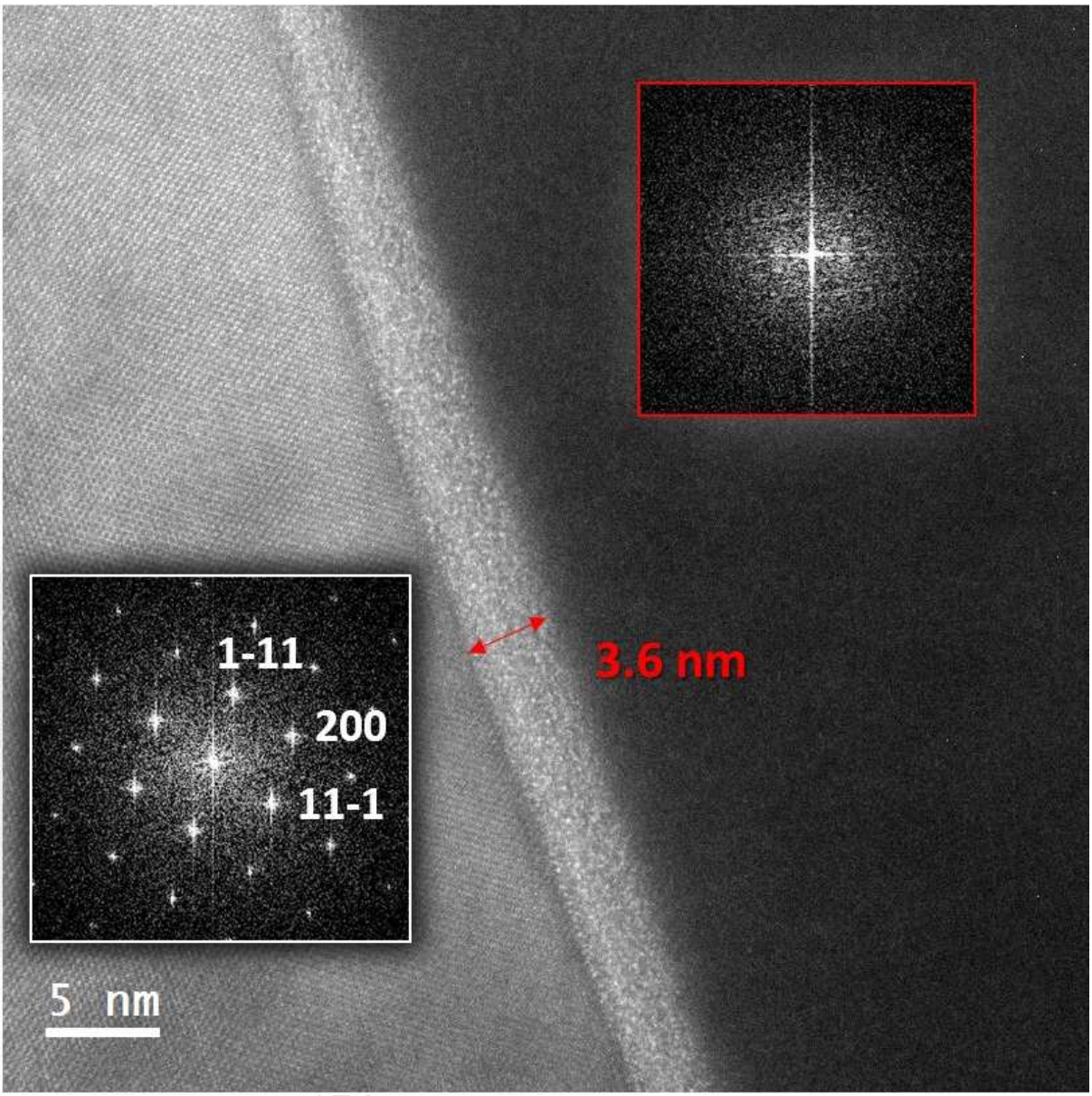

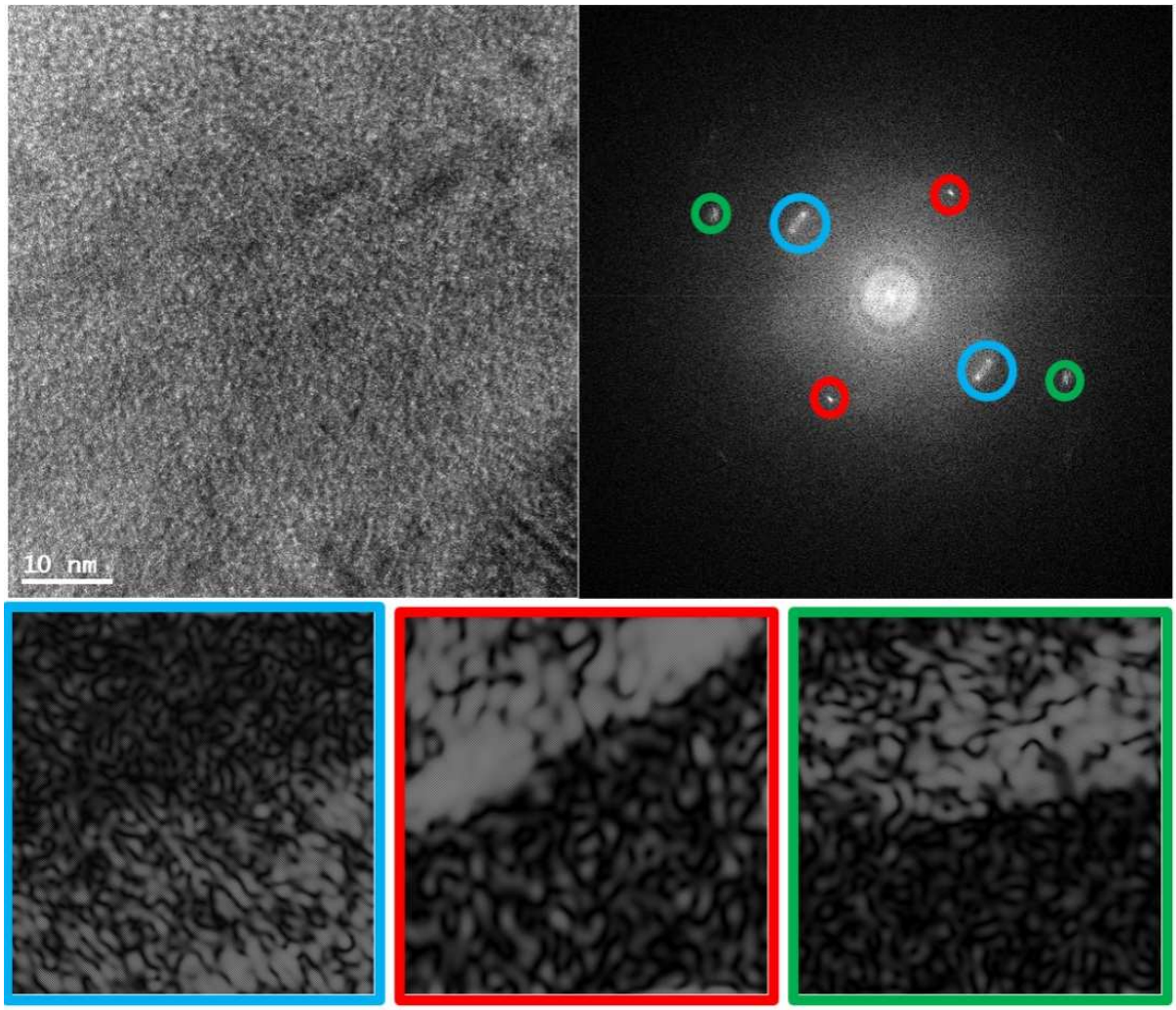

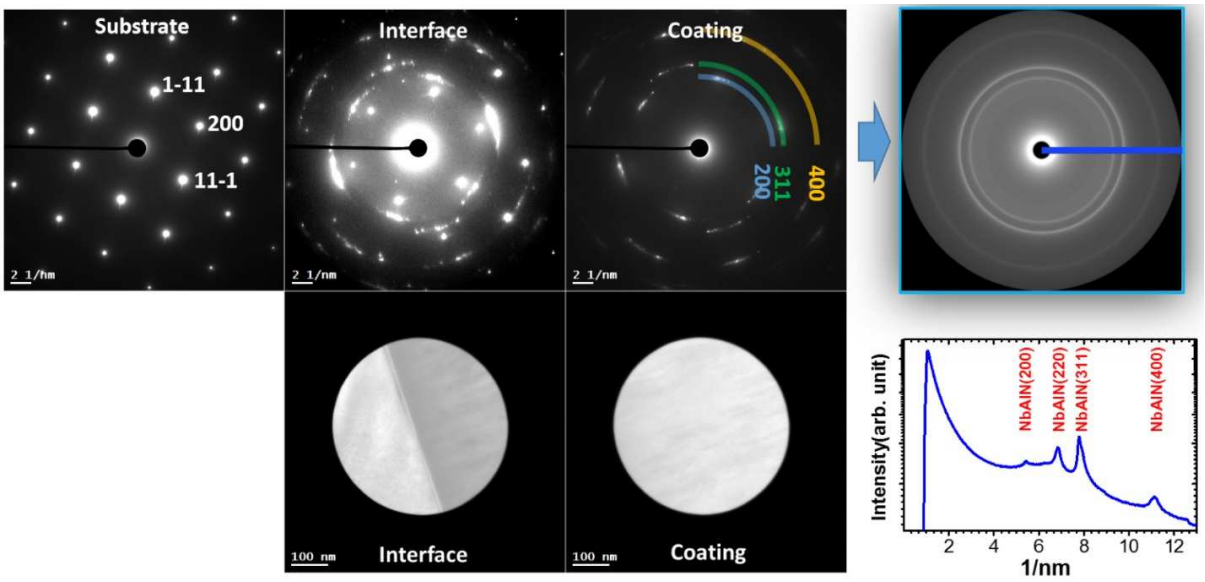

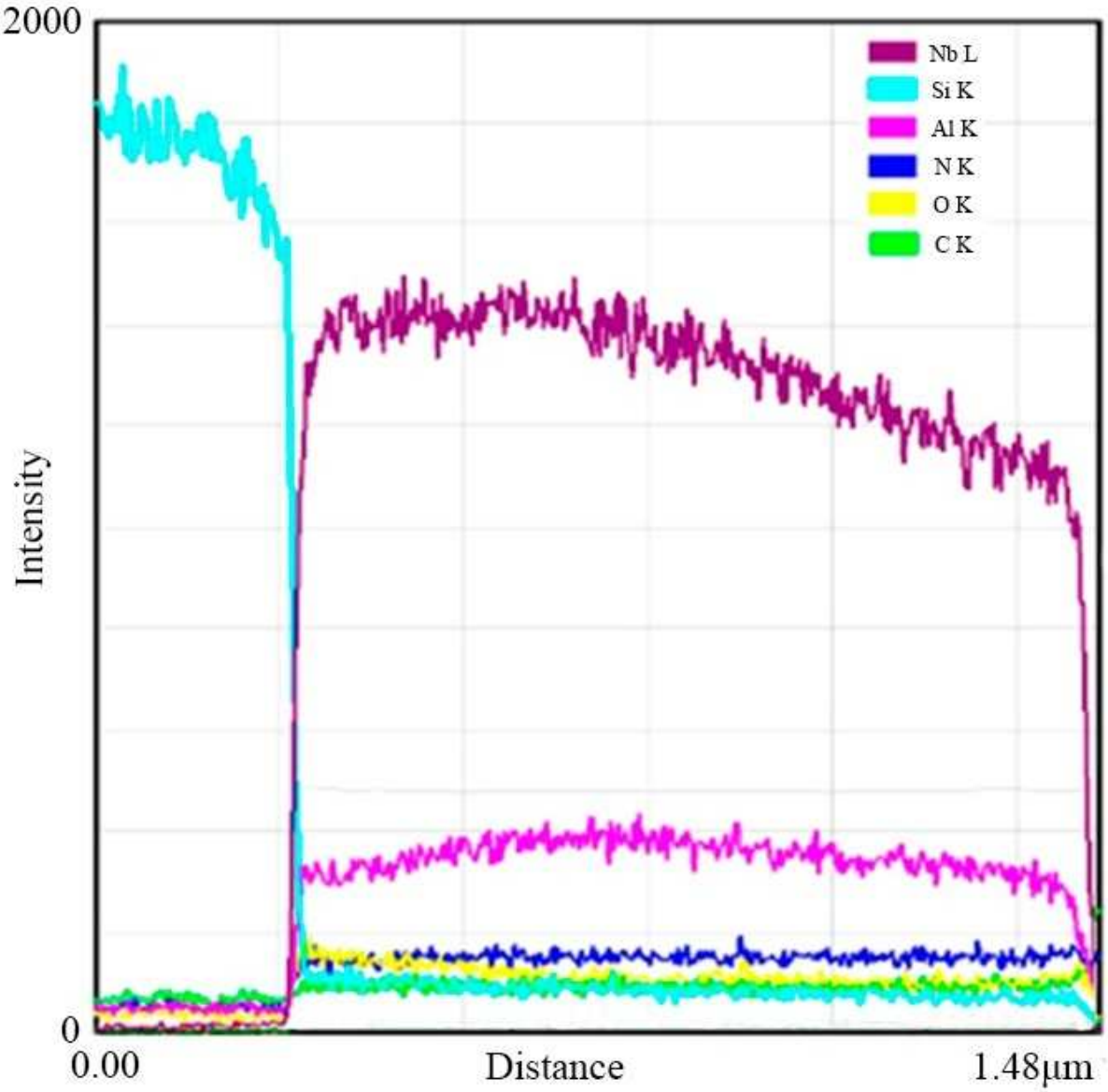

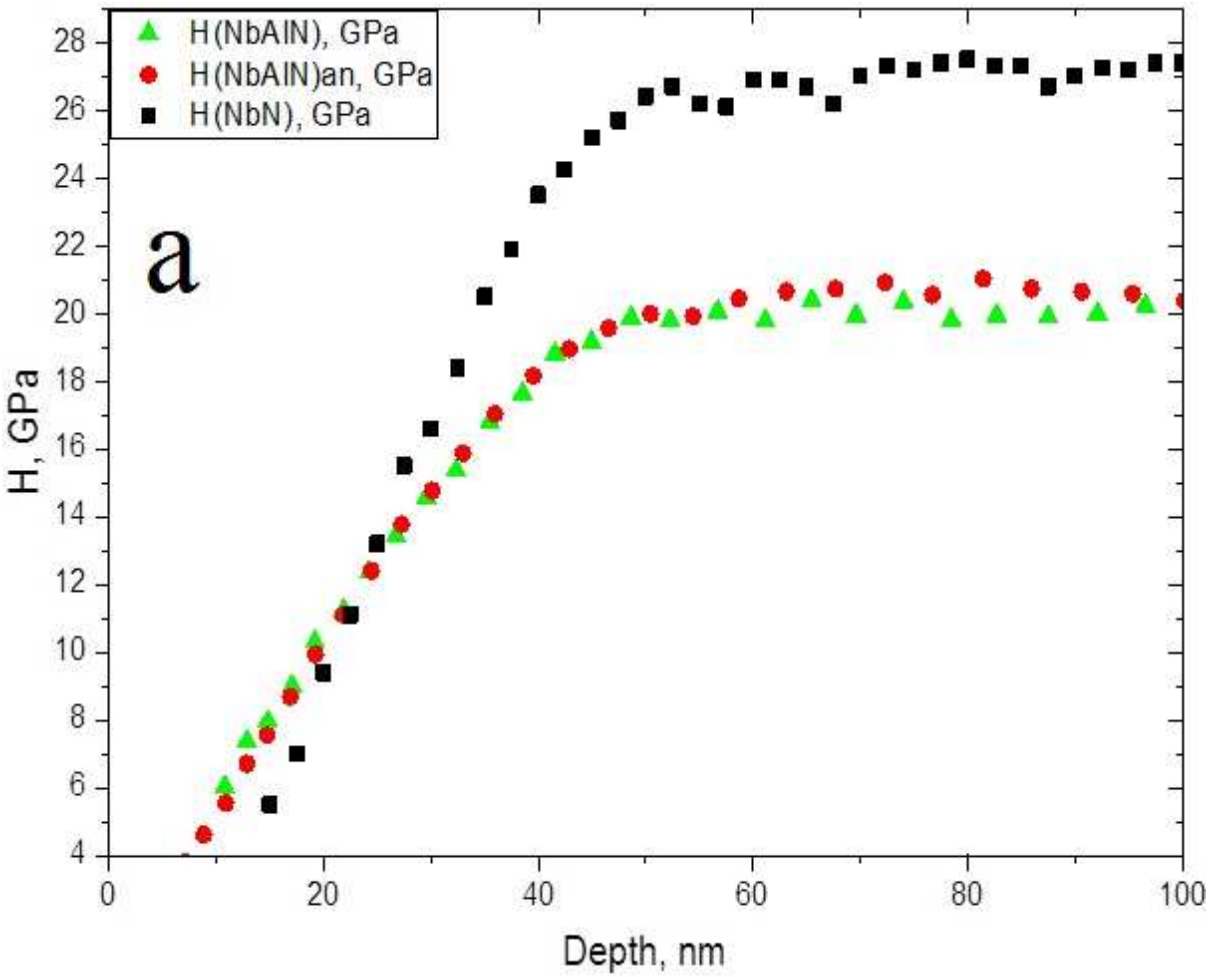
H(NbAlN), GPa
H(NbAlN)an, GPa
H(NbN), GPa
a
H, GPa
Depth, nm
4
6
8
10
12
14
16
18
20
22
24
26
28
0
20
40
60
80
100

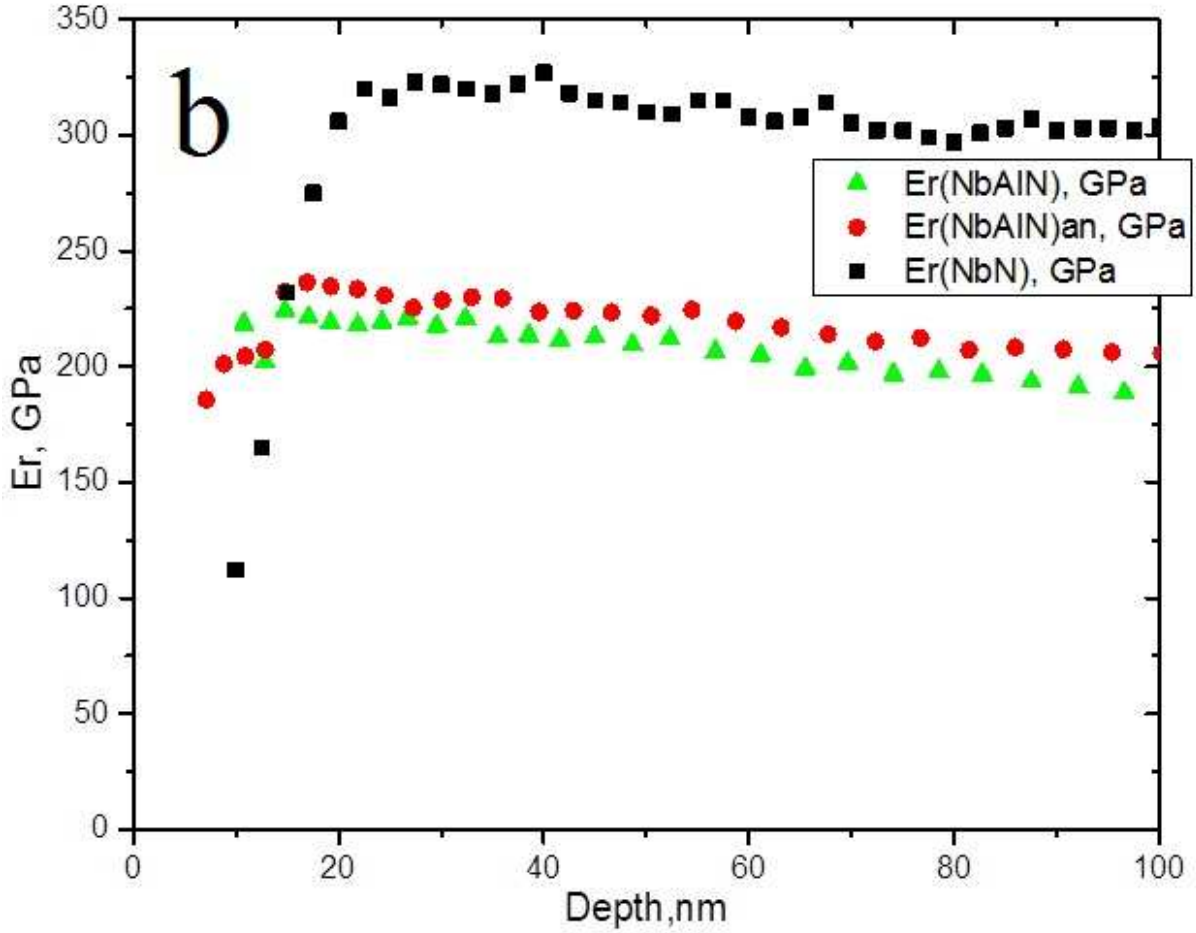

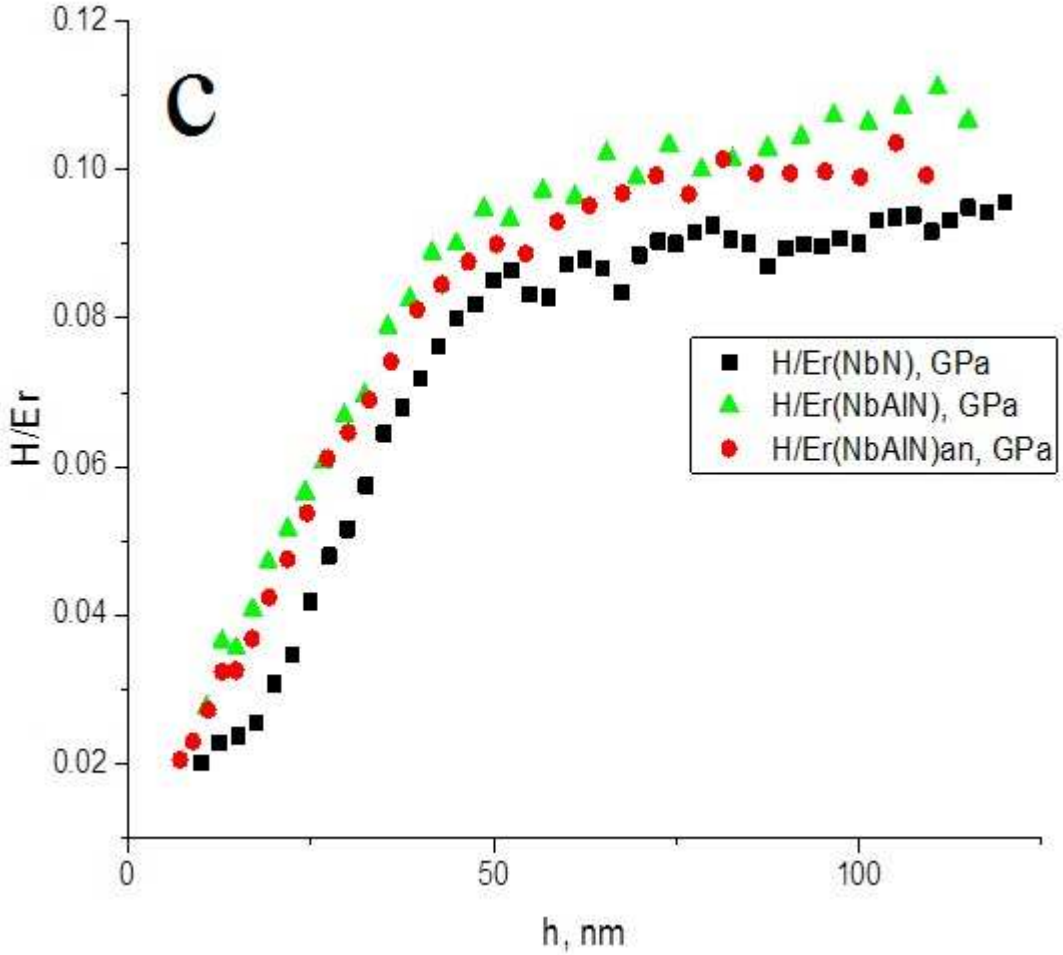
c
0.12
0.10
0.08
0.06
0.04
0.02
H/Er
0
50
100
h, nm
H/Er(NbN), GPa
H/Er(NbAlN), GPa
H/Er(NbAlN)an, GPa

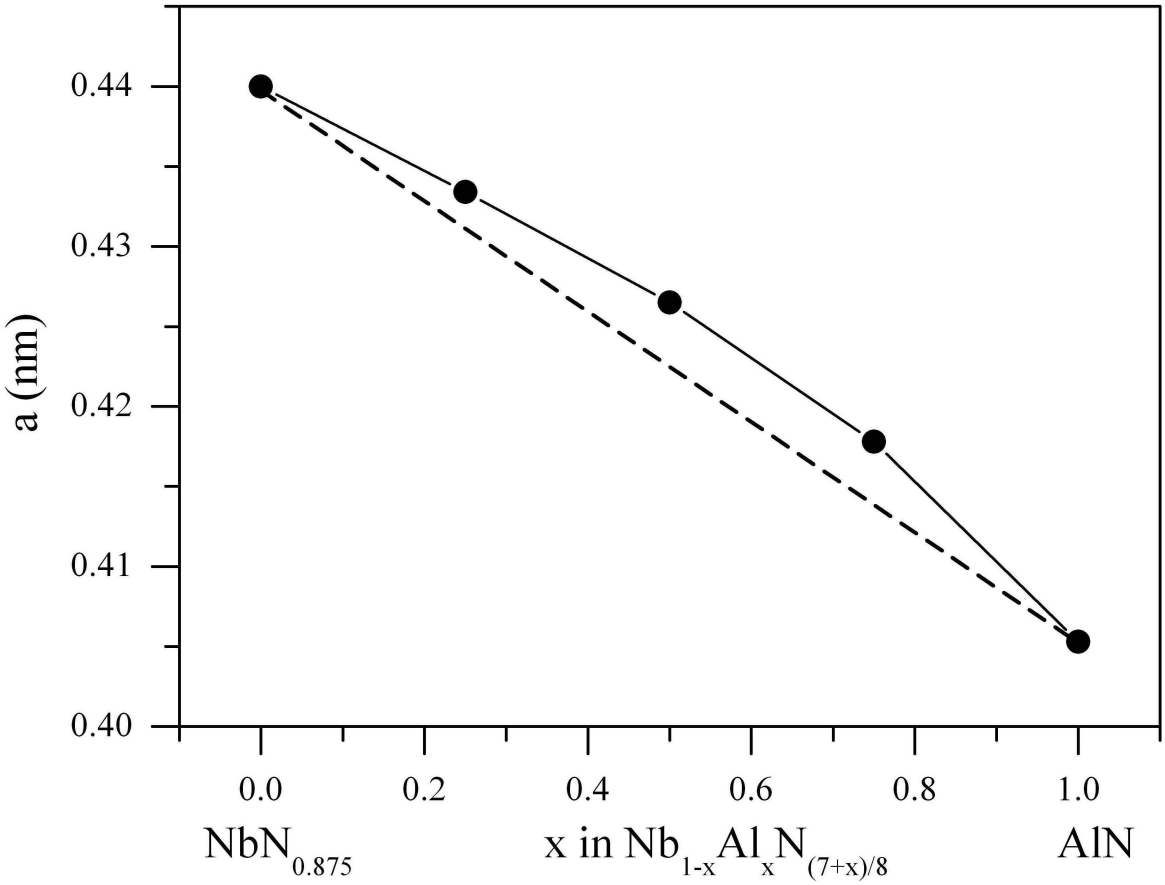

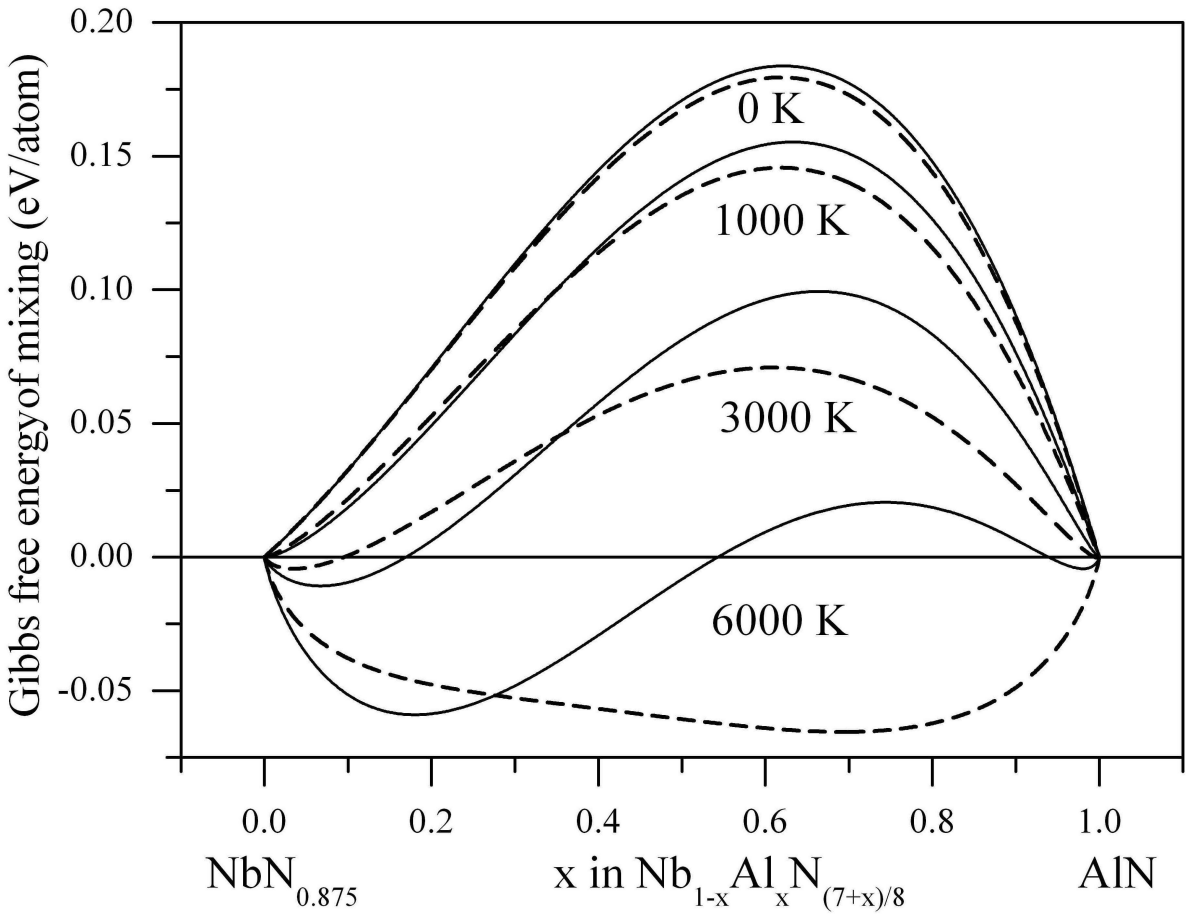

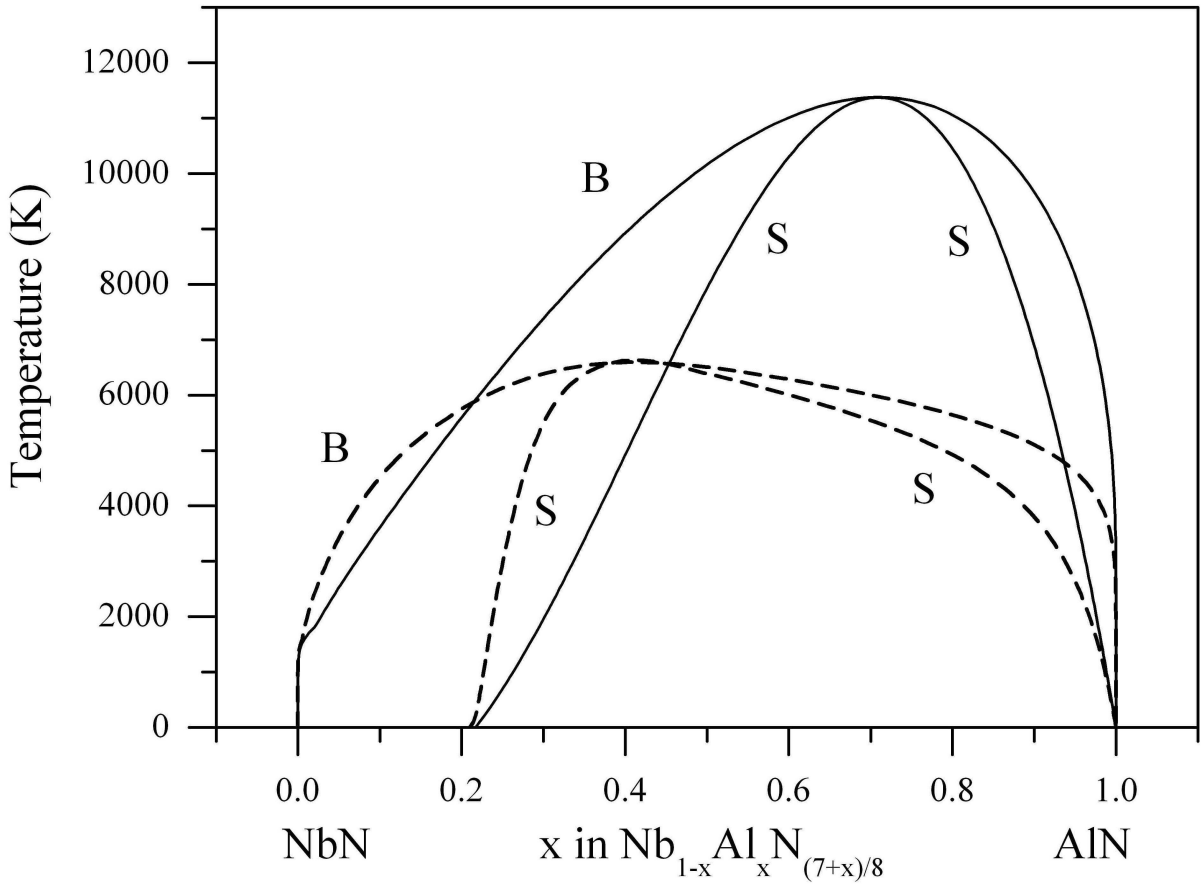

Highlights

- Nb-Al-N coatings were deposited using magnetron sputtering on silicon substrates
- Different phase transformations were observed depending on the Al content
- First-principles investigation of Nb-Al-N solid solutions was carried out
- Nanocomosite structure depends on spinodal decomposition of Nb-Al-N solid solutions
- Deposited coatings have good resistance to high-temperature annealing

Nanocomposite Nb-Al-N coatings: Experimental and theoretical principles of phase transformations [Текст] / A. Pogrebnjak, V. Rogoz, V. Ivashchenko [та ін.]
// Journal of Alloys and Compounds. — 2017. — №718. — С. 260-269.